OPTICAL DESIGN OF A THERMAL INFRARED IMAGER FOR A MICRO-SATELLITE

A THESIS SUBMITTED TO
THE GRADUATE SCHOOL OF NATURAL AND APPLIED SCIENCES
OF
MIDDLE EAST TECHNICAL UNIVERSITY

BY

ESEN SALÇIN

IN PARTIAL FULFILLMENT OF THE REQUIREMENTS
FOR
THE DEGREE OF MASTER OF SCIENCE
IN
PHYSICS

JULY 2006

Approval of the Graduate School of Natural and Applied Sciences

Prof. Dr. Canan Özgen
Director

I certify that this thesis satisfies all the requirements as a thesis for the degree of Master of Science.

Prof. Dr. Sinan Bilikmen
Head of Department

This is to certify that we have read this thesis and that in our opinion it is fully adequate, in scope and quality, as a thesis for the degree of Master of Science.

Assoc.Prof. Dr.Akif Esendemir
Supervisor

Examining Committee Members

Assoc. Prof. Dr. Serhat ÇAKIR (METU, PHYS) _____

Assoc. Prof. Dr. Akif ESENDEMİR (METU, PHYS) _____

Prof. Dr. Mehmet PARLAK (METU, PHYS) _____

Dr. Ziya Gürkan FİGEN (TÜBİTAK) _____

Assoc. Prof. Dr. Enver BULUR (METU, PHYS) _____

I hereby declare that all information in this document has been obtained and presented in accordance with academic rules and ethical conduct. I also declare that, as required by these rules and conduct, I have fully cited and referenced all material and results that are not original to this work.

Name, Last name : Esen , SALÇIN

Signature :

ABSTRACT

OPTICAL DESIGN OF A THERMAL INFRARED IMAGER
FOR A MICRO-SATELLITE

Salçın, Esen
M.S.., Department of Physics
Supervisor: Assoc. Prof. Dr.Akif Esendemir

July 2006, 85 pages

Space-based infrared Earth observation systems provide a unique opportunity for the detection of thermal variations on Earth's surface or atmosphere. The objective of this study is to propose an optical design of a thermal imager that is suitable for flight on a micro-satellite platform at an altitude of 650 km, providing the necessary resolution requirements under the considerations of physical boundaries of the given platform. Before the optical design, the parameters which would strictly bound the optical system such as the infrared source, atmospheric transmission, the detector and optical materials for infrared as well as the working conditions for the micro-satellite were examined. Simulations and further optimization efforts resulted with a high performance optical system design.

Keywords : Optical Design, Micro-Satellite, Infrared Imaging

ÖZ

MİKRO UYDU İÇİN TERMAL-KIZILÖTESİ GÖRÜNTÜLEYİCİ
OPTİK TASARIMI

Salçın, Esen
Yüksek Lisans, Fizik Bölümü
Tez Yöneticisi: Doç. Dr. Akif Esendemir

Temmuz 2006, 85 sayfa

Uzaydan, kızılötesi yer görüntüleme sistemleri, dünya yüzeyinde veya atmosferde oluşan termal değişim ve eğilimleri analiz etme imkanını vermektedir. Bu çalışmanın amacı, 650km yörünge yüksekliğindeki bir mikro-uydu için, fiziksel sınırlamaların dahilinde, gerekli çözünürlük ihtiyaçlarına cevap verebilen bir kızılötesi görüntüleyicinin optik tasarımını yapmaktır. Optik tasarımdan önce, optik sistemi sınırlayacak kızılötesi kaynak, atmosferik geçirgenlik, dedektör ve kızılötesi bölgede kullanılabilecek optik malzemeler ve uydu çalışma ortamının getirdiği gereksinimler incelenmiştir. Benzetişimler ve eniyileme çalışmaları ile yüksek performans optik sistem tasarımı sunulmaktadır.

Anahtar kelimeler : Optik Tasarım, Mikro Uydu, Kızılötesi Görüntüleme

To Mom and Dad

ACKNOWLEDGMENTS

I would like to express my deepest gratitude and thanks to my supervisor Assoc. Prof. Dr.Akif Esendemir for his guidance, advice, encouragement and friendship throughout this study. He is a great person to work with and I could never thank him enough for all that he has done.

I would like to thank Mr. Namık Açan for his assistance, suggestions and comments.

I am very grateful to my roommate Yücel Cengiz Özer, for his support (7/24), patience (I can be troublesome sometimes) and encouragement (remember our days of G.A.S.). Nothing can repay him.

I also thank Mustafa Sivaslıgil for the interpretation of atmospheric data and his useful discussions.

Special thanks to my dear friends; İnci Yıldız, for her understanding love and encouragement, Sami Kama for his discussions, valuable suggestions and providing me the documents I needed, my neighbors Nader Ghazanfari and Selçuk Yerci for their worthy supports. All of them were always ready to offer help whenever needed.

A deep sense of appreciation goes to all of my family members; Nurcan, İbrahim and Kaan Salçın for providing me endless love and support I needed to achieve my goals in life. Especially my father, who was always there whenever I needed a hand. Thank you all.

TABLE OF CONTENTS

LIST OF FIGURES

FIGURE

LIST OF TABLES

TABLE

LIST OF ABBREVIATIONS

ASTER:	Advanced Space borne Thermal Emission and Reflection Radiometer
AVHRR:	Advanced Very High Resolution Radiometer
BIRD:	Bi-Spectral Infrared Detector
DLR:	German Aerospace Centre (Deutsche Forschungsanstalt für Luft- und Raumfahrt)
DOD:	Department of Defense (US)
ESA:	European Space Agency
ETM+:	Enhanced Thematic Mapper
FOV:	Field of View
GOES:	Geostationary Operational Environmental Satellite
GSD:	Ground Sample Distance
IR:	Infrared
NETD:	Noise Equivalent Temperature Difference
NOAA:	National Oceanic and Atmospheric Administration
NASA:	National Air and Space Administration
LP:	Line Pair
LWIR:	Long Wave Infrared
METİ:	Japan's Ministry of Economy and Industry
MODIS:	Moderate Resolution Imaging Spectrometer
MTF:	Modulation Transfer Function
MWIR:	Mid-Wave Infrared
NA:	Numerical Aperture

NIR:	Near Infrared
OPD:	Optical Path Difference
OTF:	Optical Transfer Function
PSF	Point Spread Function
P-V:	Peak to Valley
RL:	Rayleigh Limit
RMS:	Root Mean Square
SNR:	Signal to Ratio
SWIR:	Short Wave Infrared
TM:	Thematic Mapper
THEMA:	Thermal High Resolution Earth Mapper
TIR:	Thermal Infrared
USGS:	The United States Geological Survey
US:	United States
UV:	Ultra Violet
VIIRS:	Visible Infrared Imager Radiometer Suite
VIS:	Visible
VLWIR:	Very Long Wavelength Infrared

LIST OF SYMBOLS

w	One detector element width
$f/\#$	F-number
T_B:	Background Temperature
ΔT :	Small Change in Temperature
F_1, F_2	First and Second Focal Points
F	Effective Focal Length
f_1	Focal length of primary mirror
d	Distance from primary to secondary mirror
s_2 , s_2'	Object and image distance
D_1, D_2	Diameter of primary and secondary mirror
C_1, C_2	Curvature of primary and secondary mirror
R_1, R_2	Radius of curvature of primary and secondary mirror
H_1, H_2	First and Second Principal Points
N_1, N_2	First and Second Nodal Points
m	Magnification
h	Image height
n	Index of refraction of optical material
d_{dif}	Diameter of the Airy disk
σ	Coddington shape factor
dn/dt	Thermorefractive coefficient
α	Absorption coefficient of an optical material

τ	Transmission through an optical element
r	Uncoated reflection loss percentage per surface
κ	Conic constant
ε	Eccentricity of conic surface
e	Clearance distance
P	Petzval radius
$D_{F.S.}$	Field stop
$E_X P$	Exit Pupil
$E_n P$	Entrance Pupil
U_p	Half Field Angle
B	Linear blur spot size
β_{spher}	Angular spherical aberration
β_{coma}	Angular coma
β_{asti}	Angular astigmatism
v_{cutoff}	Cutoff frequency
$I_{\max}$	Highest irradiance reading in the bar image
$I_{\min}$	Lowest irradiance reading in the bar image

CHAPTER 1

INTRODUCTION

1.1 Infrared Earth Observation

The infrared is part of the electromagnetic spectrum with wavelengths ranging from about 1μm to 1000μm (1mm). There are various names for the various parts which have been defined by the spectral transmission of the atmosphere and the spectral sensitivity of the detectors and are used differently by different people [1]. Since the terminology is aim dependent, it is useful to present the nomenclature used in this study.

Table1.1 Spectral Nomenclature

Visible (VIS)	400-700 nm
Near Infrared (NIR)	700-1000 nm
Short Wave Infrared (SWIR)	1-3 μm
Mid Wave Infrared (MWIR) First thermal imaging band	3-5 μm
Thermal Infrared (TIR) Long wave infrared (LWIR) Second thermal imaging band	8-12 μm
Very Long Wavelength Infrared (VLWIR)	>15 μm

The infrared spectrum has provided a rich, available technology for the accomplishment of many important and practical tasks. It has been used for many different scientific, military, forensic, civilian, industrial, astronomical and microscopic applications [1]. As one of these different applications, this study is concerned with space-based infrared Earth observation.

The rapid progress of space and infrared imaging technologies over the years has led to a new combined technology with the capability of developing impressive optical systems to acquire images in space. The infrared Earth observation data set provides a unique service for those wishing to analyze trends or rapidly detect anomalous changes in the infrared characteristics of Earth's surface or atmosphere (e.g. fire detection) [2]. By mapping thermal variations, on-orbit TIR imaging radiometers can provide a significant amount of information regarding the temperature and emissivity profiles of the ground scene [3].

Current space missions, such as MODIS, demonstrate the various applications that make use of infrared data that interest many different user groups such as; atmospheric data (atmospheric profiles, aerosol properties, ozone, cloud properties like temperature and top altitude), land data (land surface temperature and emissivity, thermal anomalies, fires and biomass burning, vegetation cover conversion), ocean data (ocean aerosol properties) that will improve our understanding of global dynamics and processes occurring on the land, in the oceans, and in the atmosphere[4]. The 20+ year legacy of space-based TIR Earth observation has in fact, encouraged the growth of numerous applications and a sizable user community who are continually developing new ways to exploit the unique characteristics of this new waveband [3].

Up to now, there have been various missions accomplished that involved space based infrared Earth observation. A list of instruments which includes the most commonly utilized by the published TIR remote sensing user community is presented [3].

Table 1.2 TIR Instruments with High Spatial but Low Temporal Resolution [3]

Instrument, (Owner), Date Launched	TIR Wavebands	GSD	Swath Width/Revisit Time	NETD @300K	Total Instru-ment Mass	Total Instrument Size
TM (USGS & NASA) 1984	10.42- 12.50μm *+6 non-TIR bands*	120 m	185 km/ 16 days	< 0.5K	425 kg	196 x 114 x 66 cm^3 (1.5 m^3)
ETM+ (USGS & NASA) 1999	10.42- 12.50μm *+7 non-TIR bands*	60m	185 km/ 16 days	< 0.5K	425 kg	196 x 114 x 66 cm^3 (1.5 m^3)
ASTER (NASA& METI) 1999	8.13- 8.48μm 8.48- 8.83μm 8.93- 9.28μm 10.12- 10.95μm 10.95- 11.65μm *+9 non-TIR bands*	90m	60km/ 46 days	< 0.3K	421 kg	73 x 183 x 110 cm^3 (1.5 m^3)
VIIRS (NOAA, NASA, DOD) 2005	3.61- 3.79μm 3.97- 4.13μm 8.40- 8.70μm 10.26- 11.26μm 11.54- 12.49μm 3.55- 3.93 μm 10.50- 12.40μm *+6 non-TIR bands*	800 m 400 m	3000 km / 0.5 day	< 0.12K	199kg	198 x 87 x 129 cm^3 (2.22 m^3)
BIRD (DLR) 2001	3.4- 4.2 μm 8.5- 9.3 μm *+2 non-TIR bands*	290 m	148 km	Not available	26 kg	~0.05 m^3

Table 1.3 TIR Instruments with Low Spatial but High Temporal Resolution [3]

Instrument, (Owner), Date Launched	TIR Wavebands	GSD	Swath Width/ Revisit Time	NETD @300K	Total Instru-ment Mass	Total Instrument Size
AVHRR (NOAA) 1998	3.55-3.93μm 10.3-11.3μm 11.5-12.5μm	1.1 km	3000km/ 0.5 days	< 0.12K	32 kg	80 x 36.5 x 29 cm^3 ($0.09\,m^3$)
ATSR ATSR-2 (ESA) 1991& 1995	3.55-3.85μm 10.5-11.5μm 11.5-12.5μm *+ 4 non-TIR bands*	1 km	500 km/ 6 days	SST <0.5K LST <0.1K	98 kg	~ $0.75\,m^3$
AATSR (ESA) 2002	3.55-3.85μm 10.5-11.5μm 11.5-12.5 μm *+4 non-TIR bands*	1km	500km/ 6days	SST <0.5K LST <0.1K	101 kg	~ $0.75\,m^3$
MODIS (NASA) 1999	3.66-3.84μm 3.93-3.99μm 1.02-4.08μm 4.43-4.49μm 4.48-4.55μm 6.54-6.90μm 7.18-7.48μm 8.40-8.70μm 9.58-9.88μm 10.78-11.28μm 11.77-12.27μm 13.19-13.49μm 13.49-13.79μm 13.79-14.09μm 14.09-14.39μm *+21 non-TIR bands*	1km	2300 km/ daily	< 0.05K	229 kg	104.4 x 118.4 x 163.8 cm^3 ($1.6\,m^3$)
GOES (NOAA& NASA)	3.8-4.0 μm 5.8-7.3 μm 6.5-7.0 μm 10.2-11.2 μm 11.5-12.5 μm 13.0-13.7 μm *+1 non-TIR band*	4 km	Full Earth Disk/ 30min	<0.1K	Not availa ble	~0.6 m^3

1.2 Objective of the Study

The objective of this study is to propose an optical design for an infrared imager for a micro-satellite assumed to be at an altitude of 650 km with a mission of observing thermal changes on Earth's surface. As a case study, early detection of forest fires was assigned as the particular aim.

Satellites that are below 100 kilograms are defined as micro-satellites. The idea behind the selection of a micro-satellite as the platform for the optical payload is the fast and cheap development, and the high performance to cost ratio with respect to larger satellites. Small missions are further characterized by a large amount of flexibility and response to new scientific opportunities. Hence, micro-satellites provide the ideal opportunity to test new systems in space within a short timeframe and low budget [5, 6].

The optical system is one of the components which make up the infrared system, as seen in Figure 1.1. If we consider the infrared source (i.e., Earth) and the transmission system (i.e., atmosphere) as the two components that we cannot intervene and assume limited detector technologies, the optical system can be thought as the most flexible component in this manner.

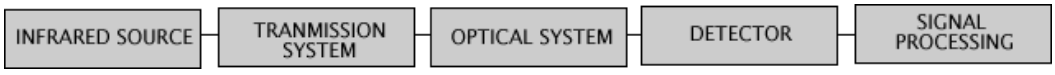

Figure 1.1 General Infrared System Layout

This correlation with other components makes the optical system a dependent variable. Hence, optics must be treated in the final stage, after the examination of all the other components.

1.3 Structure of the Study

The structure of this study can be described in three basic parts:

The first part (chapter 2) begins with the investigation of the geometry. The required ground sample distance, ground coverage, briefly the spatial resolution requirements as well as the temporal, spectral and radiometric resolution for such a task has been defined. The physical constraints of a micro-satellite have also been examined.

The second part (chapters 3, 4, 5) deals with the aforementioned components of the infrared system. The first component, the infrared source and the atmospheric effects have been considered. With the help of an atmospheric spectral transmission and radiance modeling tool; MODTRAN, the atmospheric transmission and the infrared radiance that will effect the flux reaching the satellite platform have been evaluated.

As the second component, the general considerations of the optical system was explained. This included the limited optical materials for the infrared band, thermal effects, reflection losses and coating issues. At the end, an optimum configuration selection was done by taking into account these and also the working conditions of a micro-satellite. The aim of selecting a configuration is to provide a starting point prior to initiating the design effort.

The last component, detector, has been overviewed from an optical standpoint. The type of a detector that would best suit this mission, number of pixels and the pixel sizes that the detector should possess has been discussed from an optical view.

In the third part (chapters 6, 7), the optical system design as well as the simulations and analysis were made. With the initial parameters obtained from the previous chapters, a simple code was written in MATLAB, a mathematical tool, which assisted in the listing of possible values of optical parameters that can be used in the

design. These values were examined with the help of an optical design program, ZEMAX. Further optimization efforts resulted with an optical system that revealed acceptable image quality fulfilling the requirements. Simulations and performance analysis have been made. Finally, the system has been overviewed; discussions and recommendations were made for future work.

CHAPTER 2

DEFINING REQUIREMENTS

2.1 Resolution Requirements

Imaging systems deployed on satellites provide repetitive and consistent view of the earth thus giving rise to accomplishment of broad range of applications such as;

- military surveillance and reconnaissance
- mapping
- meteorology
- agriculture
- environmental assessment and monitoring
- global change detection and monitoring
- renewable-nonrenewable source exploration
- news media

that is invaluable to monitoring the earth system and the effect of human activities on the earth [7].

These different data users have different resolution needs. Some users may require frequent, repetitive coverage with relatively low spatial resolution (meteorology). Others may desire highest possible spatial resolution with repeat coverage only

infrequently (mapping); while some users need both high spatial resolution and frequent coverage plus rapid image delivery (military surveillance) [7].

This study has an intention of designing an optical system that has a mission of observing the thermal changes on earth surface, specifically forest fires as a case study. As a preliminary step, the resolution requirements of such a system need to be defined. First of all, the concept of "resolution" has to be defined. Remote sensing systems have resolution in spectral, spatial and temporal radiometric measurement domains.

2.1.1 Spatial Resolution

Spatial resolution defines the geometric properties of the imaging system, referring to the smallest spatial element sensed by the satellite and can be described as the closest distance that two objects can be together and still be reliably distinguished [8].

When defining the spatial resolution of a sensor, the most commonly quoted quantity is the instantaneous field of view (IFOV), which is the angle subtended by the geometrical projection of single detector element on the axis of the optical system to the Earth's surface at one particular moment in time [9].

$$IFOV = 2\tan^{-1}\left(\frac{w}{2f}\right) \tag{2.1}$$

The corresponding distance on the ground is the *Ground Projected Instantaneous Field of View* (GIFOV) which is also called *Ground Sample Distance* (GSD). GIFOV depends on H, f and w. (H: altitude, f: focal length, w: detector element width). The simple geometric description is shown in figure 2.1.

$$GIFOV = 2H\tan\left(\frac{IFOV}{2}\right) \tag{2.2}$$

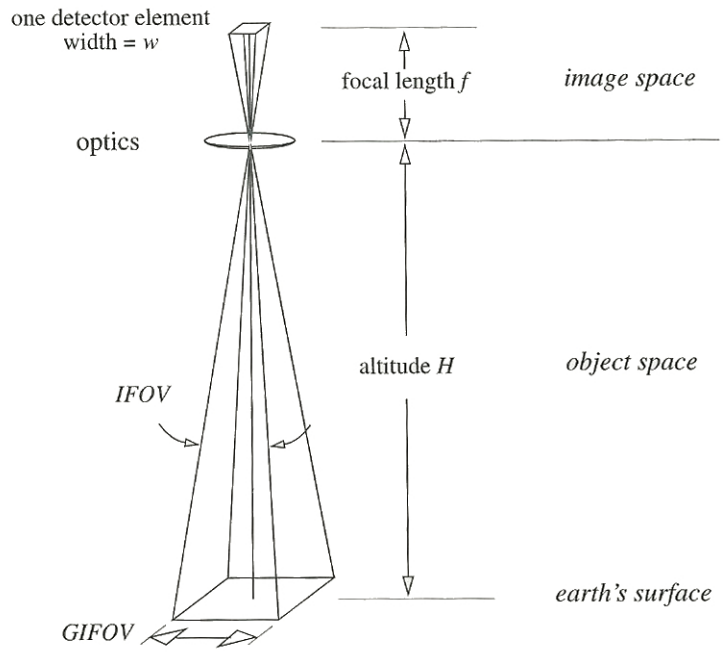

Figure 2.1 Simple geometric description of a single detector element in an optical sensor [7]

As it is clearly seen, IFOV is independent of sensor operating altitude, which makes it very convenient parameter for airborne systems where operating altitude may vary. But users of satellite data prefer to use the GIFOV (GSD) in their analysis.

The Field of View (FOV) of a sensor is the angular extent of data acquisition cross track. The corresponding cross-track ground distance is given by *

$$GFOV = 2H \tan\left(\frac{FOV}{2}\right) \tag{2.3}$$

GFOV is called the swath width-width of the terrain strip represented by the image [7]. FOV is of primary importance in any electro-optical system. A wide FOV can allow the sensor to view larger area, but the detector elements are spread over this

* The curvature of the earth is ignored.

large area yielding lower spatial resolution. In a narrow FOV, the detectors are spread over a smaller area thus increasing the spatial resolution and sacrificing area coverage, making it difficult to find objects of interest over a large area [10, 11].

Therefore, the selection of FOV is a tradeoff between area coverage and spatial resolution. The best design offers enough resolution to achieve the desired task and therefore maximize area coverage.

Careful investigation and calculation of FOV will be necessary since it will play an important part in optical design process. The FOV will be examined in detail in Chapter 6.

2.1.2 Temporal Resolution

One of the most valuable aspects of unmanned, near polar orbiting satellite remote sensing systems is their inherent repeating coverage of the same area on the Earth [7].

Temporal resolution or the revisit time defines how frequent a given a location on the earth surface is imaged at the same viewing angle a second time by the imaging system. Clearly, short revisit times are required to temporarily resolve rapidly varying target signatures. Revisit time controls how frequently the trajectory of a moving point source is sampled, an important factor in determining report time, track quality, and track accuracy [12].

The tradeoff here is between spatial and temporal resolution. Frequently sweeping large areas (high temporal resolution) with low ground sample distances (high spatial resolution) is inversely proportional.

2.1.3 Spectral Resolution

The spectral resolution describes the ability of a sensor to distinguish between fine wavelength intervals [13]. It is determined by the bandwidths of the electro-magnetic radiation of the channels used [9]. The finer the spectral resolution, the

narrower the wavelength range for a particular channel or band, providing more accurate spectral signature for discrete objects consequently the better different objects can be detected and distinguished [13].

There is a tradeoff between spectral resolution and signal to noise ratio [9]. A detector is sensitive to incoming energy over a range of wavelengths. Each of these wavelengths contributes to the signal recorded. Thus, the broader the range of wavelengths, the more energy there is available to be recorded. Thus, a broad bandwidth produces a strong signal, but a broad range of wavelengths is undesirable in that it decreases the spectral resolution i.e., the ability of the detector to assign the energy recorded to a specific wavelength [14].

Therefore, the use of well-chosen and sufficiently numerous spectral bands is a necessity, if different targets are to be successfully identified on remotely sensed images [9].

2.1.4 Radiometric Resolution

The radiometric resolution or radiometric sensitivity of an imaging system describes its ability to discriminate very slight differences in energy. The finer the radiometric resolution of a sensor, the more sensitive it is to detecting small differences in reflected or emitted energy [15]. For infrared sensors, it is usually described in terms of an equivalent blackbody temperature (i.e., the temperature of an ideal blackbody that delivers the prescribed radiance) [11]. Formally defined, sensitivity as used here is the value of the change in a distinguishing source radiant characteristics that equals the rms value of the noise at some specified point in the imaging process. Therefore, sensitivities are called noise equivalent parameters. In thermal imaging, commonly used noise equivalent parameter is the Noise Equivalent Temperature Difference (NETD). It is the small change in the targets temperature (ΔT) against a uniform background at T_B that produces a unity ratio of peak signal to rms noise when measured at some specified point in the electronic signal processing [16].

Sensitivity and spatial resolution are related so changes in sensor resolution affect sensor sensitivity. Most of the possible changes in sensor components give conflicting changes in sensitivity and spatial resolution. For example, an increase in a sensor's focal length (with all other parameters held constant) may increase spatial resolution (see figure 2.1) and decrease sensitivity [11]. Such a parameter change can give a sensitivity and resolution relationship as shown in Figure 2.2.

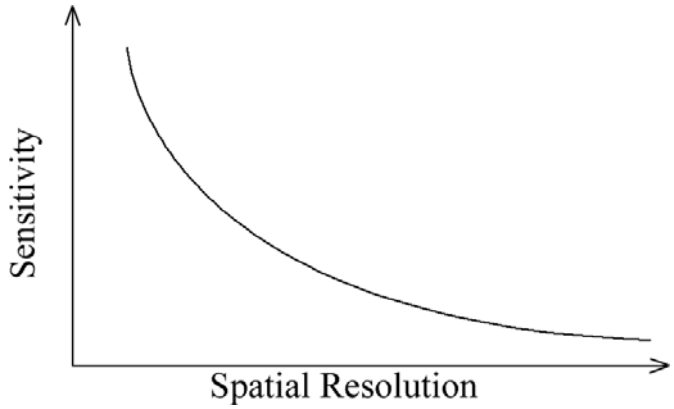

Figure 2.2 Sensitivity and spatial resolution relationship [11]

As a result, it is clear that sensor parameters involve significant tradeoffs in sensitivity, resolution, and area coverage.

As stated before, different applications need different resolution values. This study is concerned specifically with forest fires, as a case study. The required resolution for such a thermal imaging task can be determined from the previous accepted-known studies.

A list of space-borne fire recognition tasks and requirements has been presented by the German Aerospace Centre (DLR) in 2001 in the textbook "Global and Regional Vegetation Fire Monitoring from Space: Planning a Coordinated International Effort" which is listed in table 2.1 [3].

Table 2.1 Space-borne Fire Recognition Tasks and Requirements [3]

Task	Radiometric Requirements	Global requirements for global analysis		Geometric requirements for local and regional studies	
		GSD (m)	Swath (km)	GSD(m)	Swath (km)
Remote measurement of hot event temperature and area and classification of fire type	VIS, NIR; MWIR and LWIR channels: MWIR(@300K): NETD=0.5 K LWIR(@300K): NETD=0.3K	300-500	> 1500	50-100 for MWIR and LWIR	300-500

In 2003 ESA study of THEMA presented the recent and through analysis of user requirements and the general acceptance by the TIR data users [2].

Table 2.2 Sample Mission Application for TIR Earth Observation micro-satellite constellations [2]

Mission Application	GSD	NETD	Revisit Time
Thermal Trend Analysis • Forest canopy temperature • Crop hydric stress • Volcanic Plumes • Costal & Marine	 300m 200m 200m 300m	 0.1-0.3K 0.1-0.3K 0.1-0.3K	 day day day day
Thermal Change Detection • Forest Fire Detection • Volcanic Eruptions	 200m 50m	 1.5-2.5K 1.5-2.5K	 1 h week

Considering these references the spatial resolution range was determined to be 200-500m. The NETD values will play a major role in the selection of the appropriate detector. NETD range is determined to be 0.1-0.5K.

After defining the necessary spatial resolution (in terms of GSD) and radiometric requirements (in terms of NETD), major factors influencing the configuration selection (such as field of view, f-number etc.) parameters will be defined accordingly. The design and calculations are presented in chapter 6.

2.2 Micro-satellite Constraints

2.2.1 Mass Budget

Satellites are classified in terms of deployed mass. Largely, the "wet mass" of the satellite, which includes the onboard propellant, is used rather than the "dry mass" since the classification division is generally made based on launcher capabilities. Although the class boundaries are not so certain the classification is shown in Table 2.3 [5, 17].

Table 2.3 Surrey Space Centre wet mass classifications [5,17]

Class	Wet Mass (kg)
Large	> 1000
Medium	500 – 1000
Mini	100 – 500
Micro	10 – 100
Nano	1.0 – 10
Pico	0.1 – 1.0
Femto	< 0.1

So, the weight of a micro-satellite is between 10-100 kg. The allowed ratio for the payload-to-platform is generally assumed to be 20-30 %. Using the only micro-

satellite to have flown a TIR instrument as a benchmark; German Aerospace DLR's 92 kg Bi-Spectral Infrared Radiometer (BIRD) spacecraft, launched in 2001, we can conclude that a micro-satellite compatible TIR instrument should have a mass in the range of 26 kg [27, 44, 45]. The largest contributor to the mass is typically the large scanning optics and detector cooler assemblies which will need to be compact and lightweight. Therefore, deploying very long focal length or low-large aperture systems will be constrained by micro-satellites mass limitations. For this study the mass range has been determined as 2-10 kg.

2.2.2 Structure and Volume

In addition to being low mass micro-satellites tend to be fairly compact in order to withstand the launch conditions. One can see that the next generation of miniature TIR instruments should consume less than the current limit of $0.05\,m^3$ set by BIRD. From this reference, entrance aperture is chosen to be less than 100mm.

CHAPTER 3

THE INFRARED SOURCE AND ATMOSPHERIC EFFECTS

The flux emanating from the source is attenuated by the intervening atmosphere, focused on to the detector by the optical system, and then converted into a measurable electrical signal by the detector [18, 19].

The remote sensing process is bounded by the radiant energy; allowed by the atmospheric transmission. Therefore it is essential to examine the radiation reaching the satellite platform.

The primary source of infrared radiation is heat or thermal radiation, all bodies above 0 Kelvin radiate thermal radiation. This radiation of energy occurs in such a manner that can be described in terms of a blackbody emitting through a filter, making it possible to use the blackbody radiation laws as a starting point for many radiometric calculations [20]. According to blackbody model, the Earth‘s surface can be assumed as a blackbody at 300 K and the Sun at 5780 K.

A blackbody is defined as a perfect radiator which absorbs all radiation incident upon it [21]. The relation between the radiation emitted by a blackbody as a function of temperature and wavelength has been modeled by "*Planck blackbody equation*" named after Max Planck.

$$W_\lambda = \frac{C_1}{\lambda^5\left(e^{C_2/\lambda T} - 1\right)} \tag{3.1}$$

Where W_λ the radiation emitted into a hemisphere by the blackbody in power per unit area per wavelength interval ($Wcm^{-2}\mu m^{-1}$), λ = the wavelength (μm), e = the base of natural logarithms (2.718…), T = the temperature of the blackbody in Kelvin (K =°C +273), C1 = 3.742 x 10^4 and C2 =1.4388 x 10^4 when area is in square centimeters [20].

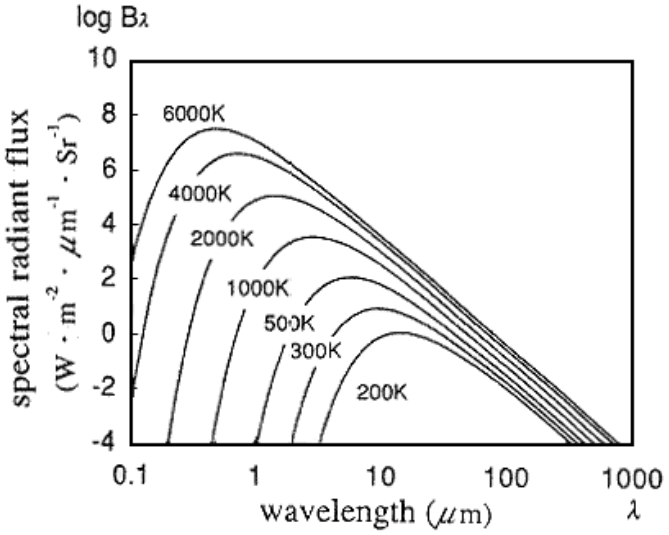

Figure 3.1 Planck's curve for several sources with different temperatures.

As it can be seen from figure 3.1, the peak of emission shifts to shorter wavelengths with increasing temperatures. The VIS, NIR and SWIR regions are the solar reflective spectral range because the energy supplied by the sun at the earth's surface exceeds that emitted by the earth itself [7]. At longer wavelengths, beyond the SWIR and into the MWIR and TIR spectral region, the effect of solar radiation declines and that of emitted thermal radiation increases. The peak wavelength of objects at terrestrial temperatures (300K) is around 9.6 μm in the LWIR band. The sun is a blackbody source with a peak wavelength of emission at 0.55 μm in the center of the human visual band [10].

The transmission of the radiation through the propagation medium; atmosphere, is another very important consideration. To assess all influences that can affect the transmission is a very complex matter. Many variables such as changes in temperature; pressure of gases; shapes, sizes and chemical compositions of suspended particles and slanted optical path for example, make it extremely difficult to predict infrared transmittance of the atmosphere [21].

The major constituents of the dry atmosphere which absorb infrared between 2-15 μm are; carbon dioxide (CO_2), methane (CH_4), nitrious oxide (N_2O), carbon monoxide (CO), ozone (O_3) and water vapor (H_2O). Ozone and water vapor vary with temperature and altitude while the others can be assumed to be permanent [21]. Ozone occurs at high altitudes (between 10 and 30 km) and is the major reason of the absorption gap between 9-10 μm (see figure 3.2).

Atmospheric transmission for a 650 km vertical path has been calculated with MODTRAN- MODerate spectral resolution atmospheric TRANSsmittance Code, a program that can model atmospheric transmittance and radiance for frequencies from 0 to 50,000 cm^{-1} at moderate spectral resolution. Model parameters include latitude/longitude, time of day, time of year, cloud conditions, view angles and lengths, and air temperature [22]. The results are shown in Figure 3.2 for 3 different geographical and seasonal models.

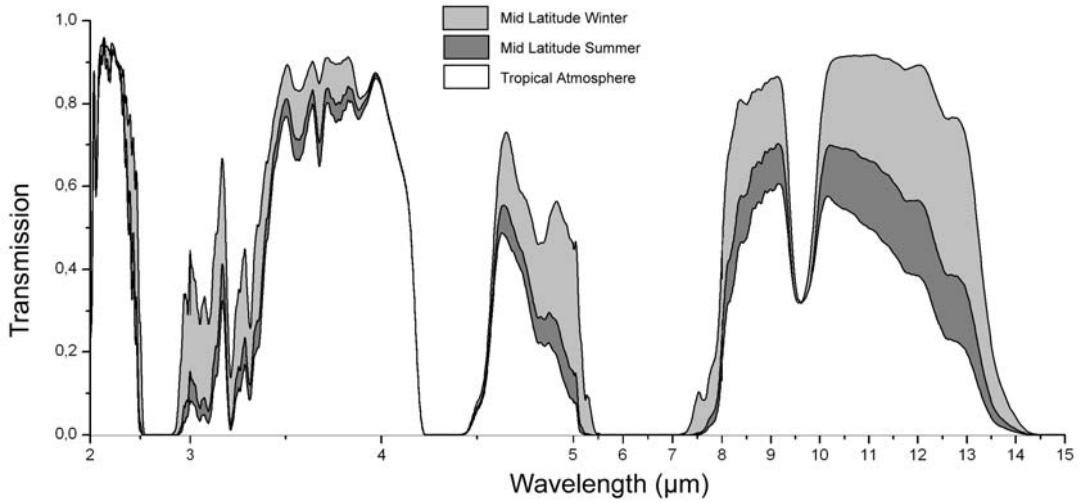

Figure 3.2 Atmospheric transmission for different seasonal and geographical models

Atmospheric transmission is one of the very important limiting factors in infrared systems as it points out the spectral intervals that can be used to extract information from a given sensor location.

It has to be stated that the total spectral radiance reaching the satellite platform, which we assume to be at 650 km altitude, is not in a form of blackbody radiation multiplied by the transmission. There are atmospheric emittance factors which contribute to the total flux. To fully describe the flux on the detector, the path radiance must be taken into consideration.

Path radiance is the natural emission of radiation by atmospheric particles within a sensor field-of-view. Given a path length between a source and a sensor, the atmospheric particles in this path contribute to the total flux on the detector [11].

The total radiance that would be measured by the satellite sensor without external illumination in one given situation is again calculated with MODTRAN. The atmospheric spectral radiance for three different surface temperatures for the model Mid Latitude Winter with respect to wavelength is shown in Figure 3.3.

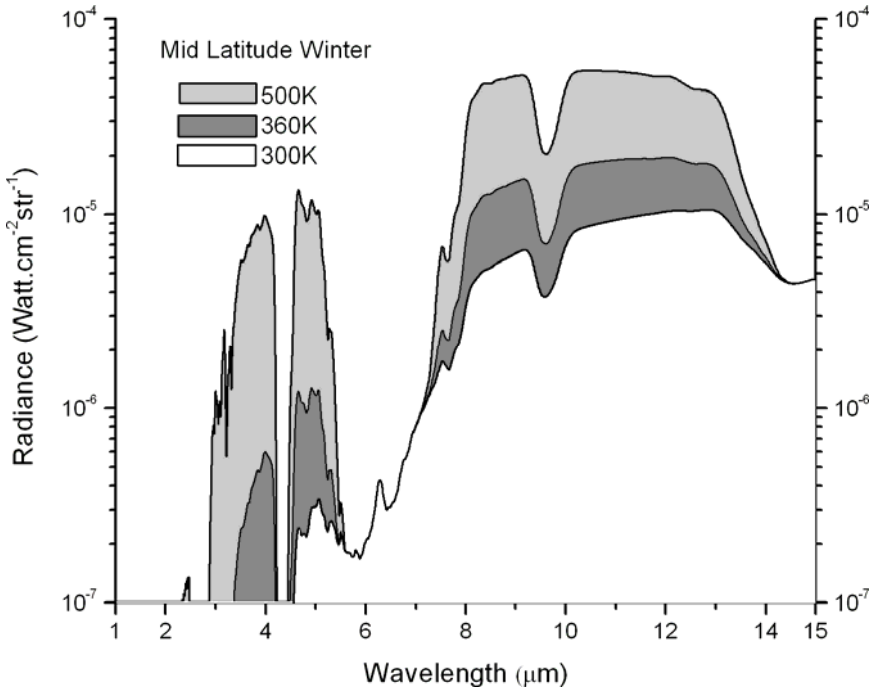

Figure 3.3 Spectral radiance for different ground temperatures.

Ignoring reflection, an imager sensitive to the emitted radiation will indicate the temperature of the scene, hence the term *thermal imager*. The efficient thermal imager therefore must be sensitive to that part of the spectrum which is emitted by material at the temperature of the scene [23].

It is clearly seen from figure 3.3 that as the temperature increases the spectral radiance in the 3-5 μm region increases dramatically. Therefore for high temperature systems, operating at close ranges or with hot targets, 3-5 μm spectral interval can be more suitable to work with. But to image scenes and targets with low temperatures, longer wavelengths offer greater sensitivity [23].

It should be emphasized that the appropriate spectral band selection can not be correctly made by these graphs alone. What is important is the SNR. If the noise is smaller or the quantum efficiency is higher, an MWIR system can perform as well as LWIR system [24].

After the examination of figure 3.3, band pass filters are determined to be used in the spectral interval of 8.13–9.30μm to 10.3–12.5μm. Thus, noise will be decreased to some amount and spectral resolution will be increased.

CHAPTER 4

OPTICAL SYSTEM

The optics of an imaging infrared or electro-optical system collects radiation from a scene and project an image of the scene onto the system detector array [11]. The size of this projected point source on the array effects the overall system performance. The actual size of the imaged point source is determined primarily by the inevitable diffraction effects set by nature and the geometrical blur caused by aberrations. The challenge in the design of an optical system is to minimize these aberrations while decreasing the f-number and maximizing the resolving power for the desired task, while maintaining good area coverage and minimizing system complexity and weight. Therefore, the assessment of diffraction and aberration effects is of uttermost importance and will be examined throughout this chapter.

4.1 Aberration Theory

The basic relationship by which the passage of light rays are traced through optical systems can be expressed by Snell's law, which describes the deviation of a ray going from a medium with any index of refraction n_1 to a another medium with a different index n_2 [20, 25].

$$n_1 \sin\theta_1 = n_2 \sin\theta_2 \tag{4.1}$$

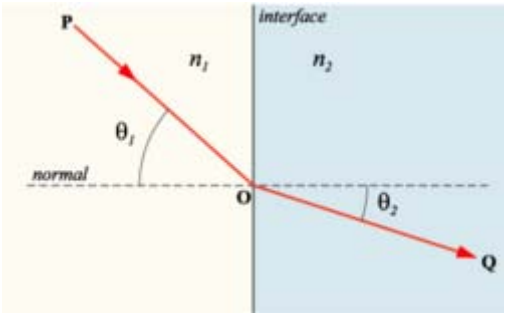

Figure 4.1 Refraction

Where n_1 and n_2 are the refraction index of the media, θ_1 is the angle of incidence and θ_2 is the angle of refraction. An expansion of the sine of an angle by infinite Taylor series gives;

$$\sin\theta = \theta - \frac{\theta^3}{3!} + \frac{\theta^5}{5!} - \frac{\theta^7}{7!} + \frac{\theta^9}{9!} \cdots \tag{4.2}$$

Rays for which angles are small enough to permit setting the cosines equal to unity and the sines and tangents equal to the angles are called paraxial rays and the infinitesimal threadlike region about the optical axis is known as the paraxial region [26, 20].

Therefore, for paraxial rays where θ is small, we may make an approximation and write $\sin\theta = \theta$ and the equations obtained by these substitutions are called first-order theory [26].

These equations are completely accurate only for paraxial region so first-order (or Gaussian) optics is often referred to as the optics of perfect optical systems. The value of first-order expressions lies in the fact that a well-corrected optical system will follow the first-order expressions almost exactly and also that the first-order image positions and sizes provide a convenient reference from which to measure departures from perfection [20].

However, in a real system, the angles of incidence are nearly always so large that the paraxial approximation is invalid and this causes the rays not to converge to a single point image [27]. The inclusion of higher-order terms, in the approximation for $\sin x$ in the series, predicts increasingly larger departures from "perfect" imaging with increasing angle. These departures are referred to as aberrations [28].

The inclusion of the next term θ^3 in $\sin\theta$ expansion results in third-order aberration theory. There will also be fifth-order aberrations as well as seventh, ninth, and higher exponents. The third and fifth order are frequently referred to as primary (or Seidel) and secondary aberration, respectively [20].

In this study we will deal only with primary aberrations. For monochromatic light there are five primary aberrations; spherical aberration, coma, astigmatism, curvature of field and distortion. An additional aberration, chromatic aberration results from wavelength dependence of the imaging properties of an optical system [28].

4.1.1. Spherical Aberration

Spherical aberration can be defined as the variation of focus with aperture. As the ray height at the lens increases, the position of the ray intersection with the optical axis moves farther and farther from the paraxial focus [20].

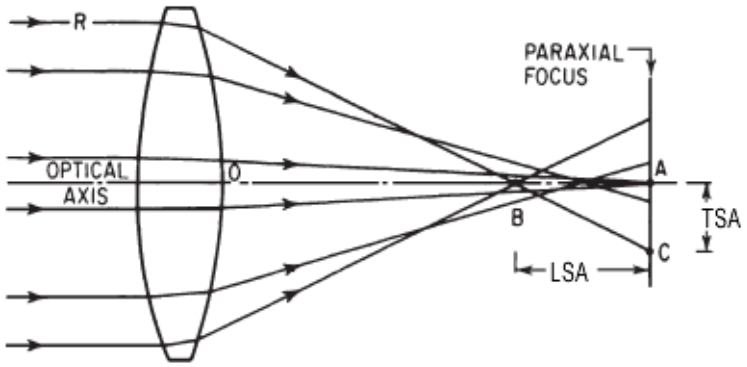

Figure 4.2 A simple converging lens with undercorrected spherical aberration. [20]

There are two possible measures of this aberration: (1) the distance between the points where the paraxial and exact rays cross the axis (longitudinal spherical aberration, or LSA)

$$LSA = L' - l' \tag{4.3}$$

And (2) the distance between the points where the rays cross the paraxial focal plane (transverse spherical aberration, or TSA) [29]

$$TSA = -LSA \tan U'_R = -(L' - l') \tan U'_R \tag{4.4}$$

l' and L' are final intercept distances of a paraxial ray and a trigonometric ray from the same axial object point. In Fig. 4.2, l' is distance OA and L' (for ray R) is distance OB. U'_R is the angle the ray R makes with the axis.

Using this sign convention, spherical aberration with a negative sign is called undercorrected spherical, since it is usually associated with simple uncorrected positive elements. Positive sign is called overcorrected spherical, generally associated with diverging elements.

For a given aperture and focal length, the amount of spherical aberration in a simple lens is a function of object position and the shape, or bending, of the lens [20]. A measure of this bending is the Coddington shape factor, defined by [28]

$$\sigma = \frac{r_1 + r_2}{r_2 - r_1} \tag{4.5}$$

where r_1 and r_2 are the radius of curvatures for surface 1 and 2, respectively.

4.1.2. Coma

In an optical system coma is defined as the variation of magnification with aperture. Rays that transmit through the lens through different portions of the aperture stop

cross the image plane at different heights from the optical axis [27]. The formation of the comatic circle is shown in figure 4.3.

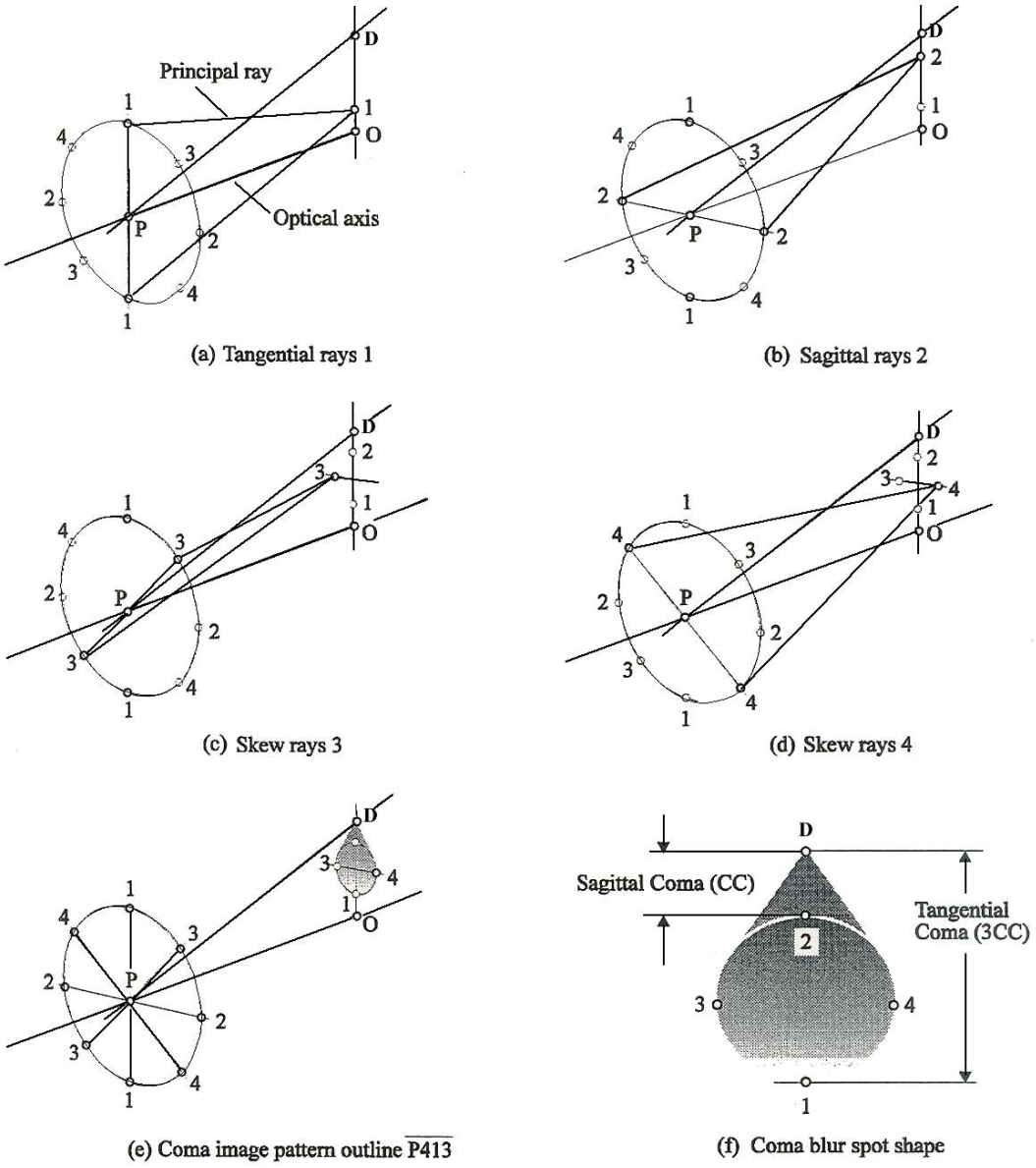

Figure 4.3 Coma [21]

PO and PD are the optical axis and the principal rays of the system. The circle marked with point pairs 1-1, 2-2, 3-3 and 4-4 is the exit pupil (E_XP) of the lens. Each circular zone of the lens forms a circular image called the comatic circle. Zone rays lying in the tangential form an image at the bottom of each comatic circle, whereas zone rays lying in a sagittal fan form an image at the top. Every other fan of rays forms images that complete the comatic circle [28]. The image pattern (f) identifies the distance D-2 as sagittal coma and D-1 as tangential coma. As noted, the tangential coma is three times the size of the sagittal coma [21]. Coma can be corrected by moving the position of the aperture stop and proper lens bending. (Eqn. 4.5)

4.1.3. Astigmatism and Field Curvature

Astigmatism occurs when the tangential and sagittal images do not coincide. In the presence of astigmatism, the image of a point source is not a point, but takes the form of two separate lines as shown in Fig. 4.4 [20]. Between the astigmatic foci the image is an elliptical or circular blur which is called “the circle of least confusion”.

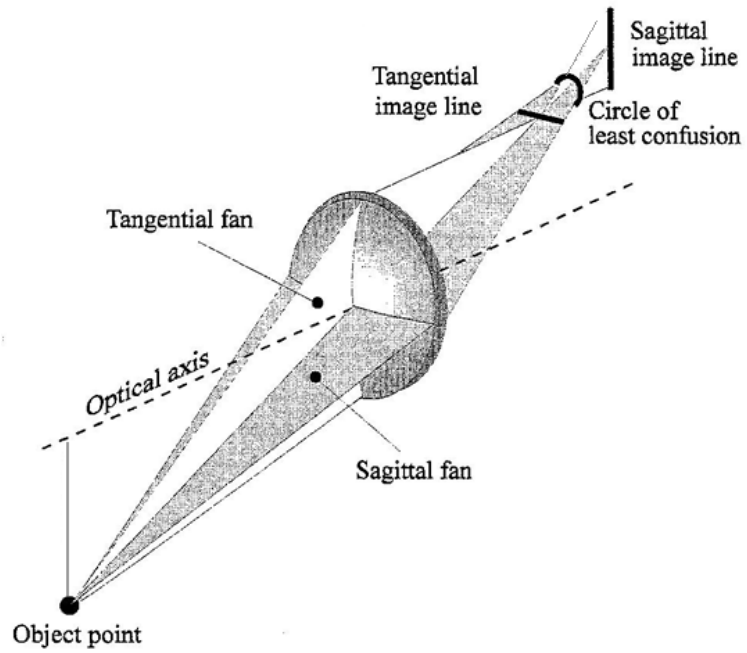

Figure 4.4 Astigmatism [21]

The elimination of astigmatism requires that the tangential and sagittal surfaces be made to coincide. When curvatures of these surfaces are changed by altering the lens shapes or distance from the aperture, so that they coincide, the resulting surface is called then Petzval surface [28]. If the surface is curved the corresponding aberration is called curvature of field. Every optical system has associated with it a sort of basic field curvature which is unaffected by the lens bending or placement and depends only on the index of refraction of the lens elements and their surface curvatures [28].

In the presence of astigmatism, both sagittal and tangential image planes are closer to the lens than the Petzval surface and the tangential image is three times further from the Petzval surface than the sagittal image according to third order theory [27].

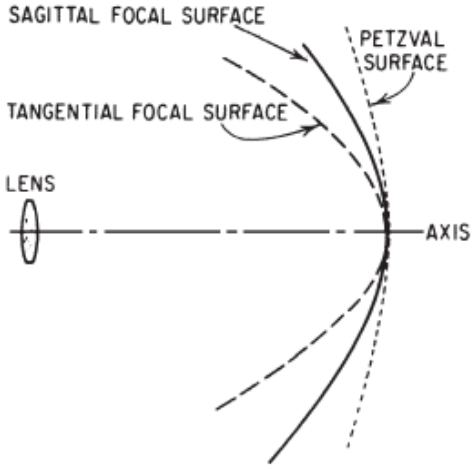

Figure 4.5 Petzval surface and primary astigmatism [20]

4.1.4 Distortion

Distortion is the variation in the magnification of the optical system with field angle [21]. When the image of an off-axis point is formed farther from the axis or closer to the axis than the image height given by the paraxial expressions, the image of an extended object is said to be distorted. The amount of distortion is the displacement

of the image from the paraxial position, and can be expressed either directly or as a percentage of the ideal image height [20].

If the magnification decreases as the distance from the axis increases, a “barrel-shaped” image occurs; if the magnification increases with distance a “pincushion” image is formed as shown in figure 4.6 [29].

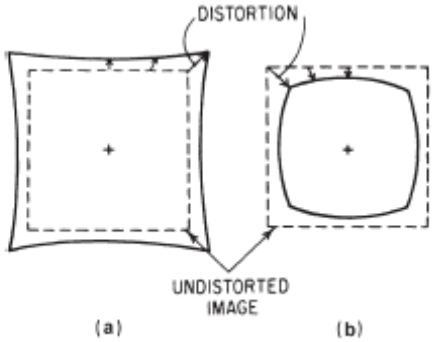

Figure 4.6 Distortion. (a) Positive, or pincushion, distortion. (b) Negative, or barrel, distortion [20]

4.1.5 Chromatic Aberration

Because index of refraction is not a constant but varies with wavelength, a lens focuses rays of different colors at different points along the optical axis [21].

In general, the index of refraction of optical materials is higher for short wavelengths than for long wavelengths; causing the short wavelengths to be more strongly refracted at each surface of a lens [20]. This defect in the lens is called *axial color*, although it occurs at off-axis points too. Axial color can be measured in terms of the distance along the axis between the two focus points, the *longitudinal axial chromatic aberration* or the distance in the focal plane as the *transverse axial chromatic aberration* [29].

Axial color is eliminated by making use of multiple refracting elements of opposite power. The most common solution is the achromatic doublet which is composed of

two elements, a positive crown (low dispersion) glass element and a negative flint (high dispersion) glass element. The crown lens is given more plus power than necessary. Flint has high dispersion that the two dispersions are then made equal but of opposite sign to cancel each other out [30].

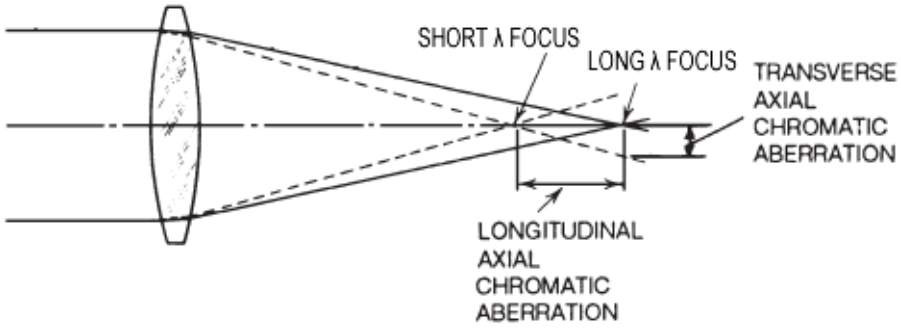

Figure 4.7 The undercorrected longitudinal chromatic aberration of a simple lens[20]

If instead of examining the distribution of rays around a focus, one examines an image point off the optical axis for a lens undercorrected for chromatic aberration the edges in the image would not be sharp but would be a blur of colors [29]. This chromatic aberration, although arising from the source as axial color, is referred to as *lateral color* or chromatic difference of magnification. This aberration is quite common in wide field-of-view systems [27]. It is the most difficult to correct, its correction may require the use of anomalous dispersion glasses, which are often expensive or diffractive elements.

4.2 Diffraction

An ideal optical system would image an object point perfectly as a point. However, diffraction occurs due to wave nature of radiation, interacting with the sharp limiting edge or the aperture of an optical system [21, 27]. Thus the point is not a point but rather a bright disk surrounded by a series of bright rings of much smaller and decreasing amplitude [31].

No matter how the lens is corrected, the result is that the actual image of a point source by a real system is a blur circle, or namely the Airy disk. If the aperture of the lens is circular, approximately 84% of the energy from an imaged point is spread over the central disk surrounded by the inner first dark ring of the Airy pattern. The remaining %16 is distributed in the rings of the pattern. The diameter of this central disk is [20, 21]

$$d_{dif} = 2.44\,\lambda\, f/\# \tag{4.6}$$

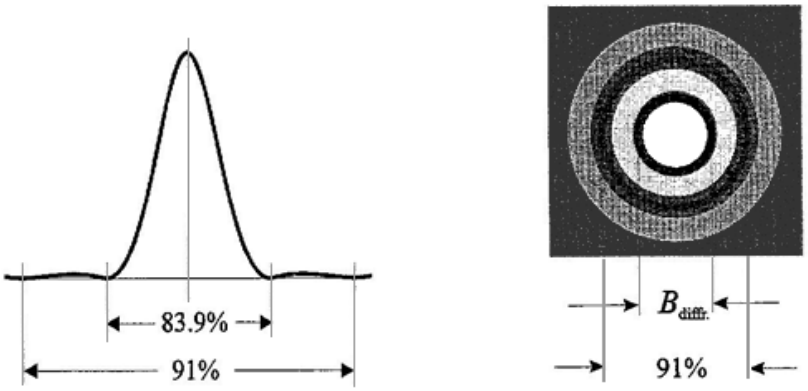

Figure 4.8. Airy disk, energy distribution and appearance [21]

If the geometrical aberrations are significantly smaller than the diffraction blur, the image is in effect well represented by the Airy disk and the system is called *diffraction-limited* [27].

The actual size of the imaged point source is determined by three contributions (1) diffraction, (2) aberrations, and (3) manufacturing defects and assembly tolerances [11].

For many optical systems, especially infrared systems where the wavelengths are much longer, diffraction produces the primary constraint on resolution because aberrations and manufacturing defects can be minimized by good optical design and tight manufacturing tolerances or alignment procedures [11].

Two separate adjacent equal-intensity point sources that are imaged very close together will form two diffraction patterns. If these diffraction patterns as in figure 4.9 are separated by the radius of the Airy disk, then the intensity midway between the two peaks in the pattern drops to 0.74 of the maximum intensity , and the two point images are said to be resolvable [27]. This is the *Rayleigh criterion* for resolution.

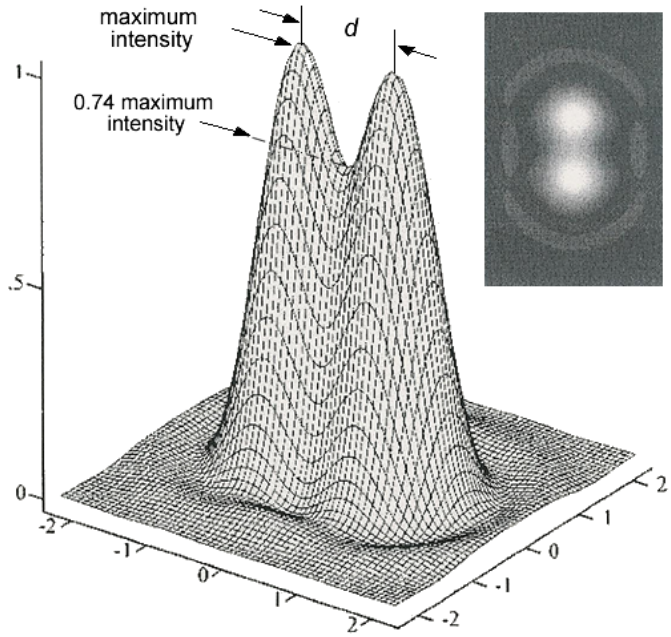

Figure 4.9. Normalized intensity patterns of two barely separated object points [31]

Rayleigh limit allows not more then one-quarter wavelength of optical path difference (OPD) over the wavefront with respect to a reference sphere. Therefore sometimes OPD in terms of its maximum departure from the reference sphere of one-quarter wavelength is used in terms of one Rayleigh limit. This is often referred to as peak-to-valley OPD [20].

Another criterion for image quality is the *Strehl ratio*. Strehl ratio is the illumination at the center of the Airy disk for an aberrated system expressed as a fraction of the corresponding illumination for a perfect system. A Strehl ratio of %80 corresponds

to a quarter-wave P-V OPD. For various amounts of OPD, the several measures of image quality are related as indicated in the following table [20].

P-V OPD	RMS OPD	Strehl ratio	% energy in Airy disk	% energy in Rings
0.0	0.0	1.00	84	16
0.25RL = λ/16	0.018λ	0.99	83	17
0.5RL = λ/8	0.036λ	0.95	80	20
1.0RL = λ/4	0.07λ	0.80	68	32
2.0RL = λ/2	0.14λ	0.4*	40	60
3.0RL = 0.75λ	0.21λ	0.1*	20	80
4.0RL=λ	0.29λ	0.0*	10	90

Figure 4.10 Relation of image quality measures [20][*]

The overall goal in high-resolution sensor design is to minimize the separation distance of two imaged point sources which equates to minimizing the diameter of the blur [11].

Therefore, one of our major aims in optical design is to minimize the diameter of the blur spot size and if possible to be in the limits of diffraction, expressed by the Rayleigh criterion. But it must be stated that in IR systems, the blur spot size is considered with the detector characteristics in mind which will be discussed in chapter 5.

4.3 Unique Features of Infrared Region

The optical design in the infrared region differs from the visible region by means of the properties of materials and the effects of the longer wavelengths [25].

For a given set of optics, resolution is much better in the visible wavelengths than in the infrared since resolution is proportional to wavelength [10]. However, it must be emphasized that higher performance is provided only if sufficient scene

[*] The smaller values of the Strehl ratio do not correlate well with image quality.

illumination is provided by the sun or other sources whereas infrared provides less resolution but performs in the absence of external illumination [10].

Further, since IR wavelengths vary many times those encountered in the visible spectrum, concepts of the particle size involved in Rayleigh and Mie scattering must be revised. Due to the fact that the amount of scattered radiation is a function of the inverse of the wavelength, infrared penetrates haze and dust much better than the visible radiation [25].

4.3.1 Optical Materials for Infrared

While there are many glass types available for visible systems, there are only a limited number of optical materials that transmit in the IR region and can be effectively used in the MWIR and LWIR spectral bands, when one considers physical characteristics, workability and cost [32, 27].

Many important properties need to be considered in the application of infrared optical materials. The selection of lens materials involves the consideration of many issues. For lenses and windows, the primary property need to be considered is the spectral region of transparency and then the index of refraction [24].

The transmission of an optical system affects the amount of flux that propagates through the system and falls on the detector. The transmission of system lenses are usually grouped into a single system optical transmission $\tau_{optics}(\lambda)$. The transmission τ through an optical element after absorption losses is expressed by exponential law of absorption:

$$\tau = e^{-\alpha x} \tag{4.7}$$

Where α is the absorption coefficient of the material and *x* is its thickness [33].

Appendix B shows some of the important properties of IR transmitting materials. It is apparent that indices of refraction are higher than they are for optical materials

in the visible. This is an advantage in the correction of third order and higher order aberrations since higher index of refraction means achieving the required ray bending [25, 33].

Other material considerations are thermal properties, elastic constants, hardness and other mechanical properties. Lens design and material selection is an extremely complicated process [11].

4.3.2 Thermal Effects

The interior of a micro-satellite encounters typically less than 10 degree C variation over an orbit [3]. Due to the thermal expansion and the change of index with refraction of the lens material with temperature, the performance of the system is affected [21].

The change of refractive index with temperature is called the thermorefractive coefficient given by dn/dt. It usually has values of about several millionths per degree, and is a function of both the wavelength and temperature [24].

The focus shift caused by the change of refractive index with temperature is a significant problem in the infrared where most refractive materials suffer from high dn/dt [32]. In order to correct this effect, mechanical or optical methods of athermalization is required.

However, for reflective optics, a uniform temperature increase or decrease will cause a uniform expansion or contraction without any induced defocus. Since this is a uniform scaling of all system parameters, the image will still be in focus [27]. Therefore reflective systems are inherently athermalized.

4.3.3 Reflectance

The transparent elements will both reflect and absorb some of the incident radiation. For radiation at normal incidence, the uncoated reflection loss per surface is expressed by the fundamental Fresnel equation,

$$r = \frac{(n-1)^2}{(n+1)^2} \tag{4.8}$$

Where r is uncoated reflection loss percentage per surface, n is index of refraction of optical material [32].

From the formula it is clear that reflection losses increase dramatically with higher index materials. For n = 4.0 reflection loss is %36! This is a vital consideration for infrared systems where high index materials are commonly used. In order to control the radiation throughoutput of an optical element antireflection coatings are essential [21].

The subject of optical coatings is very complex and extensive, therefore it is beyond the scope of this study.

For the reflective optics, metallic coatings are necessary to provide the surface high reflectivity throughout the desired spectrum. The coatings most often applied are aluminum, gold and silver, although rhodium and tantalum are sometimes used [24]. The specular spectral reflectivity representative of these coatings is given in figure 4.11.

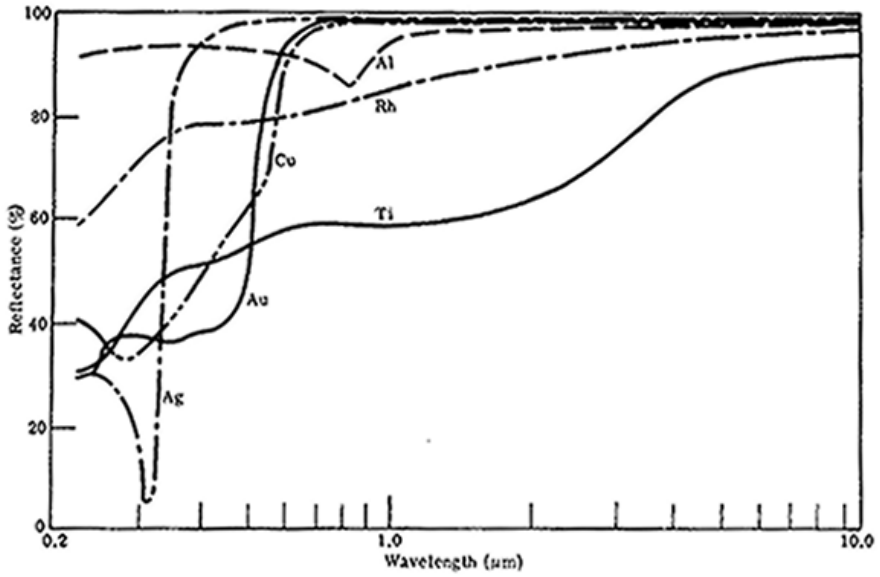

Figure 4.11 Reflectance of various films of silver, gold, aluminum, copper, rhodium and titanium [24]

4.4 Selection of the Design Configuration

The selection of an optimum configuration prior to initiating a design effort provides the starting point from which the design optimization proceeds. The configuration selection is driven by many factors. Considering the working conditions of a micro-satellite, the most suitable type of configuration was chosen to be a Cassegrain type of a reflective system rather than a refractive one. The reasons of selecting reflective surfaces are;

- One of the major problems in a system operating at such a wide spectral interval is achromatization. Although available refractive materials have high refraction and low dispersion (germanium, zinc selenide, etc.), there is limited choice of materials which may render it difficult to achromatize a system [34]. Mirrors have no chromatic aberrations of any kind. According to ray tracing theory and use of Snell's law, refractive index of a mirror is

-1.0 for all wavelengths [27]. For this reason reflective optics can be extremely well suited for wide-band applications [27].

- The optical-transmission characteristics of infrared glasses favor the implementation of all-reflective configurations for this spectral region [31].

- Reflective systems have the potential for being fully athermalized if manufactured of a single material, as explained in part 4.3.2.

- Reflective systems can be in many cases, be made of aliminium, which is light in weight. The mass limitations of the satellite platform can be overcome.

Of course there are also some disadvantages associated with reflective surfaces;

- There is often a central obscuration which results in a reduction of the effective light-collecting area, consequently a degradation of net photon throughoutput associated with reflective optical systems such as Cassegrain configuration.

- The small number of elements together with the baffling issues, and the fact that the mirrors get in each others way, limits the FOV of reflecting systems to be generally smaller than of the refractive systems [27].

- A Cassegrain reflective system has only two surfaces which are not enough to control aberrations, thus requiring the use of aspherical surfaces.

- Reflective systems are often faced with stray light. This stray light is often out of field light which directly or indirectly reaches the final sensor. Amount of stray light in the infrared is uttermost importance because it generates thermal noise. Therefore, IR mirror systems needs to be properly baffled to suppress unwanted stray light that may directly go through

missing both mirrors [31]. An example placement of baffles to prevent stray light is shown in Fig. 4.12 [31].

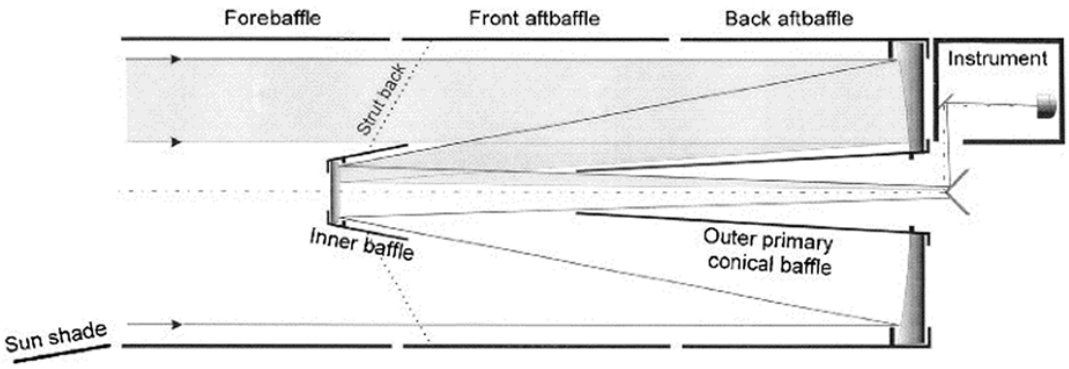

Figure 4.12 Placement of baffles to prevent stray light [31]

From various reflective types of configurations a two mirror (Cassegrain type) system is selected. A two-mirror system is the most widely used telescope configuration. It benefits from minimal reflection and central obstruction losses, is compact and offers an external and very accessible focus [35].

Table 4.1 lists the configuration of several two-mirror telescopes the types usually used in infrared systems and the aberrations that remain in the image. Each telescope consists of curved primary and secondary mirrors, folded to shorten the overall length with a hole in the primary to permit the focal point to be located behind the primary where the detectors are placed [11].

Table 4.1 Different Forms of Cassegrain Telescopes [33, 11]

Name	Primary Mirror	Secondary Mirror	Limiting Aberrations
Classical	Parabolic	Hyperbolic	Coma Astigmatism Field-Curvature
Dall-Kirkham	Elliptical	Spherical	Coma Astigmatism Field-Curvature
Ritchey-Chretien	Hyperbolic	Hyperbolic	Astigmatism Field-Curvature
Gregorian	Parabolic	Elliptical	Astigmatism Field-Curvature

Here, the conic surfaces are described by the conic constant κ as;

$\kappa = -1$	paraboloid
$\kappa < -1$	hyperboloid
$-1 < \kappa < 0$	prolate ellipsoid
$\kappa = 0$	spherical
$\kappa > 0$	oblate ellipsoid

The conic surfaces of revolution defining the mirror can be found using the conic vertex equation [35]

$$\rho^2 - 2Rz + \left(1 - \varepsilon^2\right) z^2 = 0 \tag{4.9}$$

Where R is the radius of curvature at the vertex, ε is eccentricity of the conic and ρ and z are the running surface radius and sag, respectively. κ is the conic constant and is equal to $(-\varepsilon^2)$ which defines the conic family according to [52] ;

$$z = \frac{\rho^2}{2R} + (1+\kappa)\frac{\rho^4}{8R^3} + (1+\kappa)^2\frac{\rho^6}{16R^5} + (1+\kappa)^3\frac{5\rho^8}{128R^7} + \cdots \qquad (4.10)$$

The Cassegrain configuration we have chosen consists of two surfaces which will not be enough to control aberrations, thus requiring aspherical surfaces.

CHAPTER 5

DETECTOR-FROM AN OPTICAL STANDPOINT

The detector is the heart of an imaging system because it converts infrared radiation into measurable electrical signal and target spatial information into electrical temporal information [18]. In this chapter the study of the detector is carried out from an optical point of view. The detailed analysis of the detector systems are beyond the scope of this study.

System resolution depends on the optical blur diameter and the detector size. When system is detector limited, small changes in the blur diameter have little effect on the system resolution. The detector size limits the smallest size that can be discerned. With a large blur diameter the resolution is limited by optics-which is often the case for a system like the one presented here [32]. A commonly used measure of optical resolution is Airy disc size, as explained in chapter 4. For a LWIR system operating at a wavelength of 12μm and an f/# of 2, the diffraction blur with %84 of the energy is 58,56μm in diameter (Airy). The trend to decrease the pixel sizes in focal plane arrays to increase the system's resolution requires awareness of this limit set by nature [21]. As the detector pixel size decreases the f-number must also decrease to match the detector. This fact plays a key role in the selection of matching pixel size.

The miniaturization trends in micro-satellites sets pronounced limitations on mass, volume, power consumption and cost. Cryogenic cooling of detectors will boost the performance level but at the expense of higher cost and complexity. Fabrication of uncooled infrared detectors based on microbolometer technology offers a low-cost thermal imaging sensor for many applications [36]. For a micro-satellite with the above mentioned thresholds, the uncooled types of thermal detectors were determined to be the most suitable for this mission.

Another advantage of thermal detectors apart from the fact of not requiring cooling and operating at room (ambient) temperature is the thermal detector's equal response to all wavelengths [11]. This contributes to the stability of a system that must operate over a wide temperature range [21].

Detectors are mostly arranged in arrays. In thermal imaging a number of detector elements are mounted in either a single line or a two dimensional layout. Linear arrays reduce the required scanning mechanism to one axis. Two-dimensional arrays eliminate scanning completely [21]. As it was mentioned in Chapter 2, one of the major contributors to volume in a micro-satellite is scanning mirrors. Therefore, a staring array type of detector was selected for such a volume-limited platform.

From an optical standpoint, however, there is a trade-off, since such an arrangement of staring arrays presents an extended FOV which leads to a higher degree of complexity with regard to aberration corrections. The FOV definition from the image space is directly proportional to the FPA sizes as seen in figure 6.1. As the FPA size increases the FOV extends proportionally, providing large area coverage on the ground, which is very desirable for short revisit times needed for detecting rapidly varying target signatures (See table 2.1 criteria). But the trade-off here is that such an extended FOV leads to large amount of off-axis aberrations like coma, distortion, lateral color which complicates the overall optical system design.

With the selection of Cassegrain type of reflective system as the design configuration in chapter 4, the FOV is rather limited considering the baffling issues, which prevents us from using large format FPA's. For this study, an uncooled FPA with 160x120 pixels and with a 46μm pixel pitch was determined to be suitable. The calculations in Chapter 6 are done using these values. It should also be noted that the NETD values of the selected detector should be in between 0.1-0.5K in order to satisfy the radiometric requirements presented in Chapter 2.

CHAPTER 6

SYSTEM DESIGN, SIMULATION AND ANALYSIS

6.1 Derivation of System Specifications

The system analysis generally refers to the task of deriving the basic optical system parameters based on the functional system performance requirements.

6.1.1 Process of the Design

The specifications that have been defined in the previous chapters can be summarized in a scheme that will also show the process for the design. As seen in figure 6.1, the design process is shown in 9 steps. The sensor requirements (step 1) and the physical limitations of a micro-satellite (step 2) have been determined in Chapter 2, which enables us to solve for the effective focal length and optical aperture diameter (step 6). From the examination of IR source and atmospheric effects (step 3) in Chapter 3, the spectral band selection is made (step 4). Then, a suitable FPA is determined (step 5) in Chapter 5 which will be used in the calculations of the necessary optical parameters (step 7) - together with steps 4 and 6. Finally, the system can be established in steps 8 and 9. In this chapter, steps 6, 7, 8 and 9 will be covered.

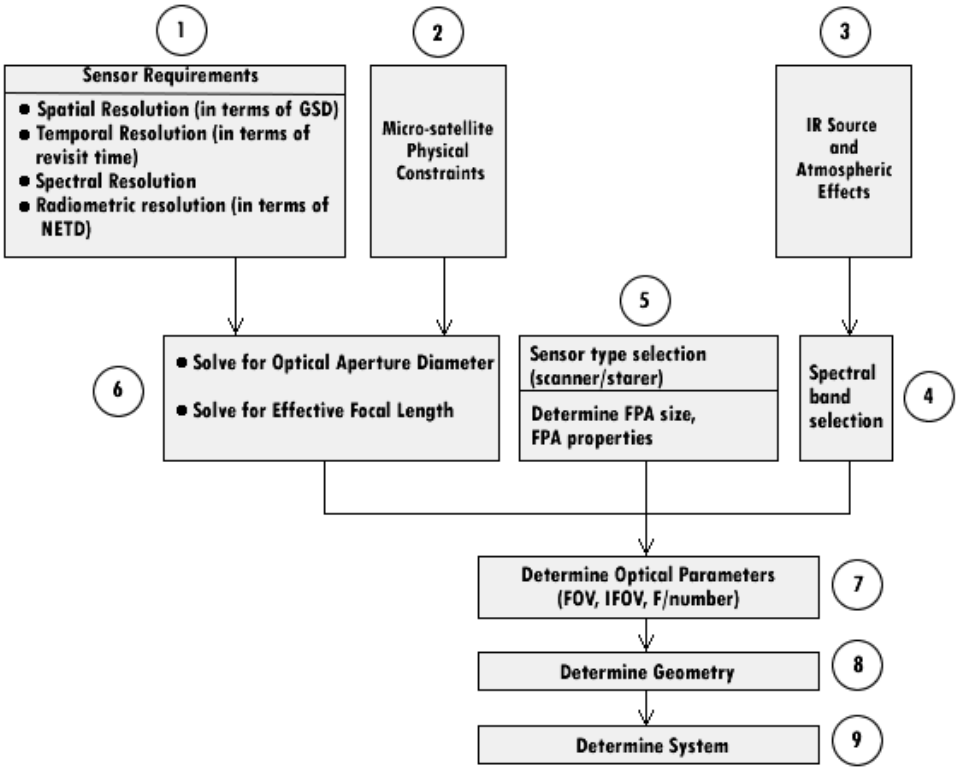

Figure 6.1 The process for the optical system design in 9 steps

6.1.2 Effective Focal Length

In Chapter 2, considering Table 2.1 and 2.2 criteria of detecting thermal changes on Earth's surface, spatial resolution range was determined to be 200-500m. With the selection of a ground sample distance value of 300 m, the satellite altitude of 650 km, one detector element width of 46μm, the required effective focal length is found to be approximately 100 mm using equations (2.1) and (2.2).

6.1.3 Optical Aperture Diameter

In Chapter 2 the volume limit was determined to be less than $0.05\,m^3$, by using BIRD as a reference for this study. The optical entrance aperture diameter is chosen to be less than 100 mm under this volume limit.

6.1.4 Field of View (FOV)

The FOV of an infrared imaging system is one of the most important design parameter. It is the parameter that describes the angular space in which the system accepts light [11].

As it can be seen from the geometrical construction in figure 6.2, the diameter of the field stop, $D_{F.S.}$ affects the FOV. If the field stop is made smaller, the FOV will be reduced accordingly. By analogous reasoning, the instantaneous field-of-view (IFOV) will be affected by the size of the individual detecting element, *d*. The IFOV is the range of incident angles seen by a single detecting element in the focal plane. (see chapter 2.2.) [37].

The detector has been chosen to be in a staring array form (see chapter 5). In this case, the size of the image plane is defined by the light-sensitive area of the array and the field stop is equal to the detector array size. A field stop larger than the detector size would not limit the FOV and hence would not be required.

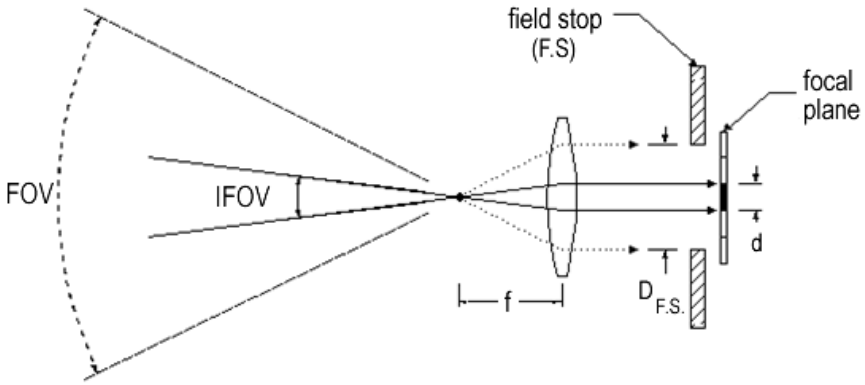

Figure 6.2 Field stop

The IFOV and FOV can be calculated using trigonometry [37]

$$IFOV = 2\tan^{-1}\left(\frac{w}{2f}\right) \tag{2.1}$$

$$FOV = 2\tan^{-1}\left(\frac{D_{F.S.}}{2f}\right) \tag{6.1}$$

The field of view for staring focal plane arrays is expressed in horizontal and vertical components, labeled as FOV_v and FOV_h respectively as shown in figure 6.3. For the systems that view objects at a range much larger than the focal length *f*, the FOV are the arctangents of the image size divided by the focal length [11, 21].

$$\mathrm{FO}V_v = 2\tan^{-1}\left(\frac{v}{2f}\right) \qquad \mathrm{FO}V_h = 2\tan^{-1}\left(\frac{h}{2f}\right) \tag{6.2}$$

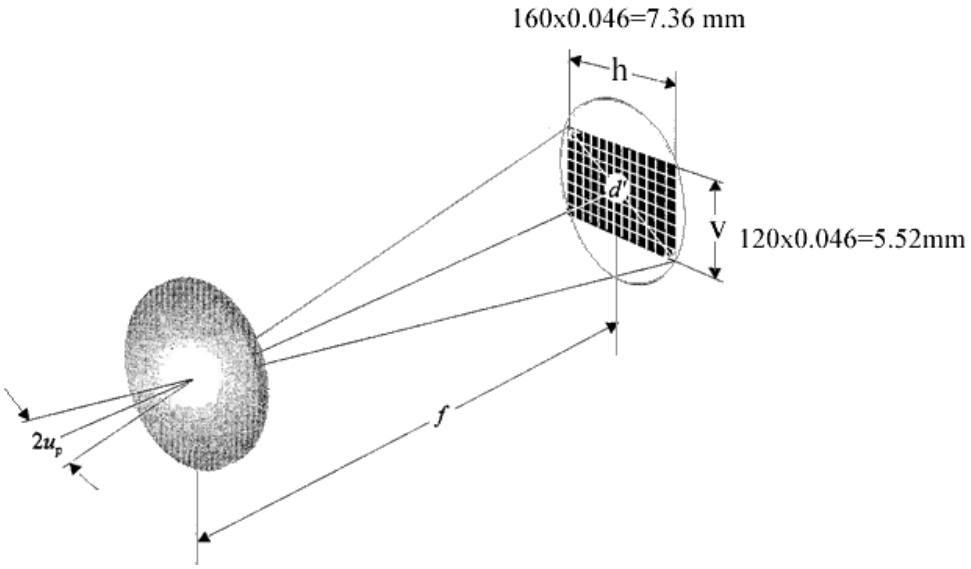

Figure 6.3 Field of view calculation

If we assume to use a 160 x 120 FPA with 46 μm pixel pitch as it was determined in chapter 5, the FOV can be calculated as;

- $\mathrm{FOV}_v = 2\tan^{-1}\left(\frac{5.52mm}{2x100mm}\right) = 3.16$ degrees
- $\mathrm{FOV}_h = 2\tan^{-1}\left(\frac{7.36mm}{2x100mm}\right) = 4.21\,\mathrm{degrees}$

Full Field of view is;

- $\mathrm{FOV}_{d'} = 2\tan^{-1}\left(\frac{9.2mm}{2x100mm}\right) = 5.26\,\mathrm{degrees}$

The IFOV is;

- $IFOV = 2\tan^{-1}\left(\frac{0.046mm}{2x100mm}\right) = 0.026$ degrees

6.1.5 Ground Coverage

Using equation 1.1;

$$GFOV_v = 2H\tan\left(\frac{FOV_v}{2}\right) = 2x(650x10^3 m)\tan\left(\frac{3.16}{2}\right) \cong 35.8\ km$$

$$GFOV_h = 2H\tan\left(\frac{FOV_h}{2}\right) = 2x(650x10^3 m)\tan\left(\frac{4.21}{2}\right) \cong 47.7\ km$$

Therefore the imager will cover approximately 36 km by 48 km on the ground.

6.2 The Design

The selection of an optimum configuration prior to initiating a design effort provides the starting point from which the design optimization proceeds [27]. Using general geometry, estimation of some optical parameters is possible which will enable us to make a reasonable selection.

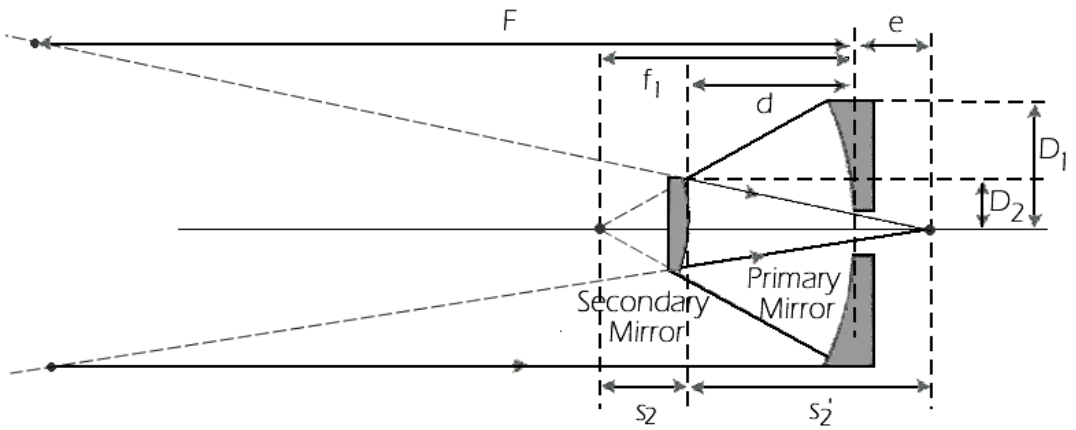

Figure 6.4 The geometry of the two-mirror Cassegrain type system

Where;

F :	Effective Focal Length
m :	Magnification
s_2 and s_2' :	Object and image distance of intermediate object (located at focal point of primary)
f_1 :	Focal length of primary mirror
d :	Distance from primary to secondary
D_1 and D_2 :	Diameter of primary and secondary mirror
C_1 and C_2 :	Curvature of primary and secondary mirror
R_1 and R_2 :	Radius of curvature of primary and secondary mirror
e :	Clearance distance
k :	Obscuration ratio
P :	Petzval radius

The effective focal length of the system can be defined as [38, 39] ;

$$F = m.f_1 = \frac{s_2'}{s_2} f_1 \tag{6.3}$$

$$D_2 = \frac{D_1}{f_1} s_2 \tag{6.4}$$

The obscuration ratio is;

$$k = D_2 / D_1 \tag{6.5}$$

From (6.3) and (6.4);

$$k = \frac{D_2}{D_1} = \frac{s_2'}{F} \tag{6.6}$$

The back focus s_2' can be expressed in terms of mirror spacing *d*;

$$s_2' = d + e \tag{6.7}$$

Mirror curvatures are [35];

$$C_1 = \frac{s_2' - F}{2.d.F} \quad \text{and} \quad C_2 = \frac{s_2' + d - F}{2.d.s_2} \tag{6.8}$$

$$R_1 = 1/C_1 \qquad R_2 = 1/C_2 \tag{6.9}$$

Petzval radius is [20,40]

$$P = \frac{s_2'.F.d}{F.d - (s_2' - F)^2} \tag{6.10}$$

The primary aberrations in angular units [21] :

Spherical aberration $$\beta_{spher} = \frac{F(b-F)^3 + b(F-d-b)(F+d-b)^2}{128.F.d^3(f/\#)} \tag{6.11}$$

Coma $$\beta_{coma} = \frac{h\left[2f(b-F)^2 + (F-d-b).(d-F-b)\right]}{32d^2F^2(f/\#)^2} \tag{6.12}$$

Astigmatism $$\beta_{asti} = \frac{h^2\left[4bF(b-F) + (F-d-b)(d-F-b)\right]}{8F^3bd(f/\#)^3} \tag{6.13}$$

where *h* is the image height and *b* is the back focal distance (s_2').

The linear blur spot size B is;

$$B = F.\sum \beta \tag{6.14}$$

To obtain a useful starting point, all of the constraints must be taken into consideration.

The initial constraint is the effect of obscuration, which primarily needs to be evaluated. The obscuration ratio must be no more than 30% [34, 31, 20, 40]. The image must be outside the primary mirror in order to place the FPA behind. Therefore the back focus (s_2') must be larger than the thickness (*d*).

With the help of a mathematical tool; a high-performance language for technical computing MATLAB; a starting solution for the initial phase of the design was obtained. The possible values are listed in Table 6.1.

These values were examined and evaluated with the help of an optical design program, ZEMAX. Among these values, a back focus of 40.00 mm, mirror spacing of 33.00mm, clearance distance of 7.00 mm with primary and secondary mirror curvatures of -93.78 and -42.58 mm, respectively, was selected.

Unfortunately, with such an arrangement the off-axis aberration correction is difficult in the given FOV using only two surfaces. A corrector element is necessary. Because the corrector is a refractive element, some chromatic aberration will be introduced. However, since the corrector is inserted close to the focal plane and its thickness is small, the effect is minimal [21].

From the examined infrared optical materials (Appendix B) very widely used, high refractive index material germanium was inserted. Germanium will both act as a corrector, a protector glass in front of the FPA and also a band pass filter to block unwanted radiation from different spectral intervals.

Table 6.5 Primary and Secondary Mirror Geometry

k	BackFocus(B)	d	e	R1	R2	PETZVAL	SUM	SPH	COMA	ASTI
0.27	37.0000	22.00000	15.00000	-60.61224	-21.42105	-16.56467	-5.52934	-7.42182	2.52074	-0.62826
	37.00000	23.00000	14.00000	-63.36735	-22.69333	-17.67733	-4.74980	-6.48503	2.33610	-0.60087
	37.00000	24.00000	13.00000	-66.12245	-24.00000	-18.83721	-4.10212	-5.69955	2.17320	-0.57577
	37.00000	25.00000	12.00000	-68.87755	-25.34247	-20.04736	-3.56010	-5.03611	2.02868	-0.55268
	37.00000	27.00000	10.00000	-74.38776	-28.14085	-22.63215	-2.71654	-3.98932	1.78440	-0.51162
	37.00000	28.00000	9.00000	-77.14286	-29.60000	-24.01442	-2.38672	-3.57398	1.68056	-0.49330
	37.00000	29.00000	8.00000	-79.89796	-31.10145	-25.46230	-2.10416	-3.21467	1.58675	-0.47624
	37.00000	30.00000	7.00000	-82.65306	-32.64706	-26.98055	-1.86090	-2.90229	1.50170	-0.46031
0.28	38.00000	24.00000	14.00000	-66.80412	-24.98630	-19.95785	-3.90746	-5.45443	2.11680	-0.56982
	38.00000	25.00000	13.00000	-69.58763	-26.38889	-21.25456	-3.38989	-4.81939	1.97647	-0.54697
	38.00000	26.00000	12.00000	-72.37113	-27.83099	-22.61061	-2.95400	-4.27947	1.85134	-0.52587
	38.0000	27.00000	11.00000	-75.15464	-29.31429	-24.03019	-2.58465	-3.81756	1.73925	-0.50634
	38.00000	28.00000	10.00000	-77.93814	-30.84058	-25.51785	-2.26993	-3.42011	1.63839	-0.48821
	38.00000	29.00000	9.00000	-80.72165	-32.41176	-27.07863	-2.00036	-3.07632	1.54728	-0.47132
	38.00000	30.00000	8.00000	-83.50515	-34.02985	-28.71804	-1.76834	-2.77744	1.46466	-0.45556
	38.00000	31.00000	7.00000	-86.28866	-35.69697	-30.44219	-1.56776	-2.51642	1.38949	-0.44082
0.29	39.00000	22.00000	17.00000	-61.87500	-23.18919	-18.54467	-5.02108	-6.79481	2.38900	-0.61528
	39.00000	23.00000	16.00000	-64.68750	-24.57534	-19.81591	-4.31007	-5.93663	2.21501	-0.58846
	39.00000	24.00000	15.00000	-67.50000	-26.00000	-21.14458	-3.71959	-5.21719	2.06148	-0.56388
	39.00000	25.00000	14.00000	-70.31250	-27.46479	-22.53467	-3.22566	-4.60966	1.92526	-0.54126
	39.00000	26.00000	13.00000	-73.12500	-28.97143	-23.99054	-2.80977	-4.09317	1.80379	-0.52039
	39.00000	27.00000	12.00000	-75.93750	-30.52174	-25.51696	-2.45746	-3.65136	1.69496	-0.50106
	39.00000	28.00000	11.00000	-78.75000	-32.11765	-27.11921	-2.15732	-3.27124	1.59703	-0.48312
	39.00000	29.00000	10.00000	-81.56250	-33.76119	-28.80306	-1.90031	-2.94246	1.50856	-0.46641
0.30	40.00000	24.00000	16.00000	-68.21053	-27.04225	-22.40277	-3.53836	-4.98766	2.00725	-0.55794
	40.00000	25.00000	15.00000	-71.05263	-28.57143	-23.89381	-3.06727	-4.40676	1.87505	-0.53556
	40.00000	26.00000	14.00000	-73.89474	-30.14493	-25.45784	-2.67071	-3.91296	1.75716	-0.51491
	40.00000	28.00000	12.00000	-79.57895	-33.43284	-28.82745	-2.04881	-3.12726	1.55648	-0.47803
	40.00000	29.00000	11.00000	-82.42105	-35.15152	-30.64579	-1.80392	-2.81302	1.47060	-0.46150
	40.00000	30.00000	10.00000	-85.26316	-36.92308	-32.56281	-1.59325	-2.53990	1.39272	-0.44607
	40.00000	31.00000	9.00000	-88.10526	-38.75000	-34.58678	-1.41121	-2.30141	1.32184	-0.43164
	40.00000	32.00000	8.00000	-90.94737	-40.63492	-36.72689	-1.25324	-2.09225	1.25712	-0.41811
	40.00000	33.00000	7.00000	-93.78947	-42.58065	-38.99344	-1.11563	-1.90808	1.19784	-0.40540
	40.00000	34.00000	6.00000	-96.63158	-44.59016	-41.39797	-0.99532	-1.74528	1.14339	-0.39343
	40.00000	35.00000	5.00000	-99.47368	-46.66667	-43.95349	-0.88977	-1.60085	1.09324	-0.38216

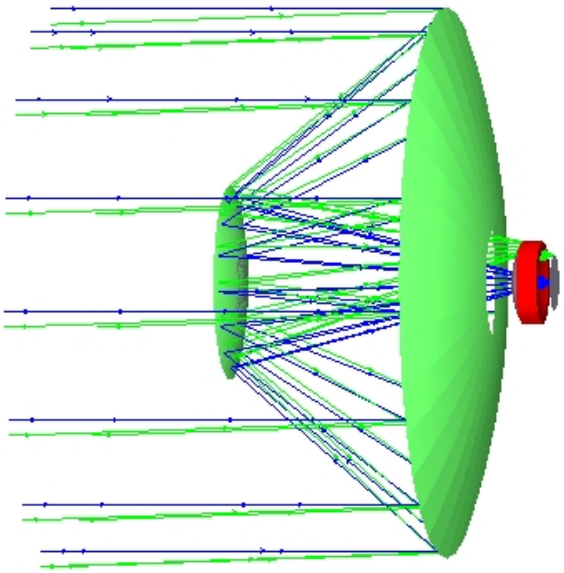

Figure 6.6 Shaded model of the designed system

After the determination of the primary parameters, the iterative process of optimization starts. The radius of curvatures, thickness, of the germanium corrector element has been calculated as presented in table 6.2.

Table 6.2 Corrector Element Data

Surface	Radius of Curvature(mm)	Thickness(mm)	Semi-aperture	Conic
1	11.25	3.00	5.25	0.00
2	9.99	-	4.10	0.00

The required aberration correction has been achieved without the need to use aspheric surfaces which are very costly and difficult to manufacture, as the conic constant is set to zero. Other calculated optical parameters are presented in Appendix C, Prescription Data.

6.3 Performance Evaluation

The results of the optical computations need to be interpreted. The basic question to which we address ourselves is “What effect does a given amount of aberration have on the performance of the optical system?”

There are many ways to measure and evaluate image quality. For the infrared the blur spot size and radial energy distribution in the image plane are two quantities of interest. They indicate the minimum detector element size required to collect certain amount of energy [21]. From this information one can derive the MTF a measure of contrast versus resolution.

6.3.1 Spot Diagrams

One set of calculations that are quite useful in evaluating a lens or an optical system consists of imposing a rectangular grid on the entrance pupil and then tracing rays from an object point to all the intersections of grid lines in the pupil [29].

Then, the intersection of each ray with the selected image plane is plotted, and since each ray represents the same fraction of the total energy in the image, the density of the points in the plot is a measure of the power density (irradiance, illuminance) in the image. Obviously the more rays that are traced, the more accurate the representation of the geometrical image becomes. A ray intercept plot of this type is called a *spot diagram* which provides insight into the performance of the optical system [20].

In the software that is used, the root-mean-square and geometric spot radius is output with the spot diagrams. The rms spot diameter is the diameter of a circle containing approximately 68% of the energy. This metric is of a great value especially when working with pixelated sensors where one often wants the image of a point object to fall within a pixel [27].

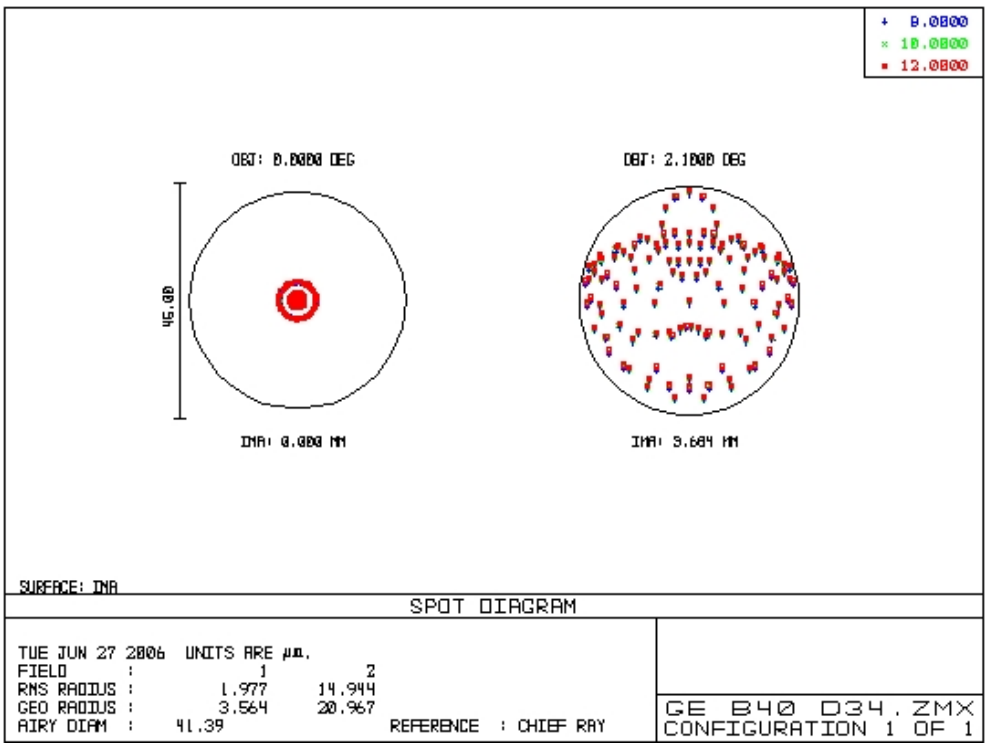

Figure 6.7 Spot Diagrams

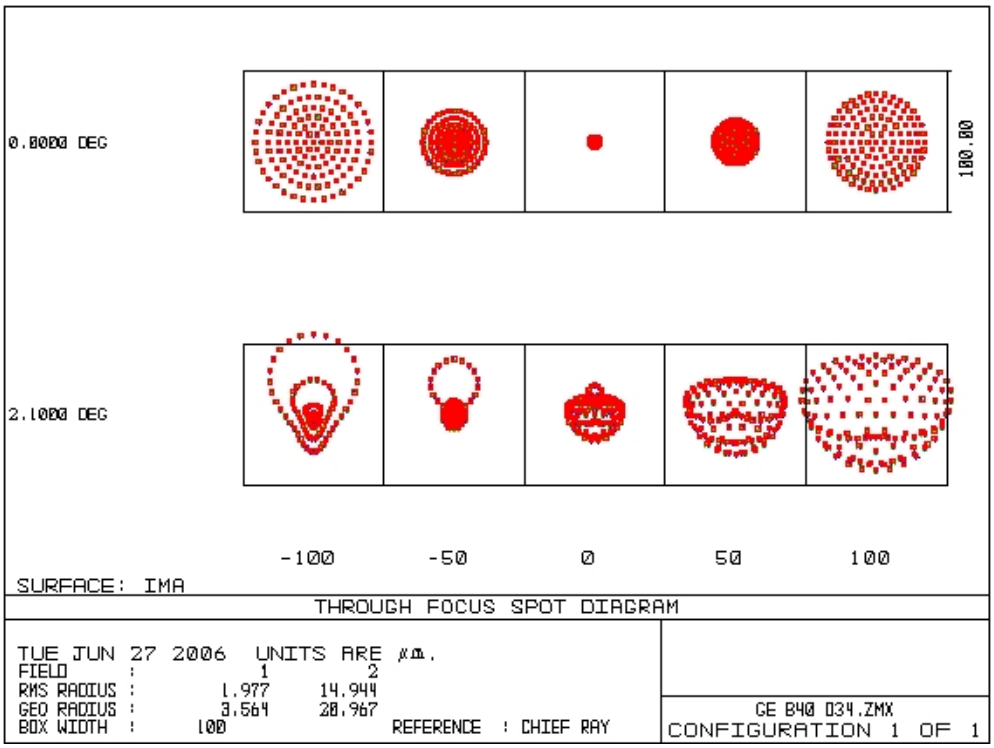

Figure 6.8 Through Focus Spot Diagrams

The spot diagrams for the design is shown in the figures 6.7 and 6.8. The airy diameter is approximately 41.4 µm for the working f/number of 1.41. This is a desirable value considering the detector pixel size of 46 µm. For the half field of 2.10 degrees the rms radius is approximately 15 µm meaning that all the rays are well within the Airy disk. The system is diffraction-limited.

6.3.2 Encircled Energy

Encircled energy is energy percentage plotted as a function of image diameter. A good reliable and simple specification is that 80% of the energy from a point object shall fall within a diameter equal to the pixel pitch of the sensor [27].

Figure 6.9 shows the encircled energy plot. 80% of energy is contained within a diameter of approximately 23 µm which is a good match to the sensor.

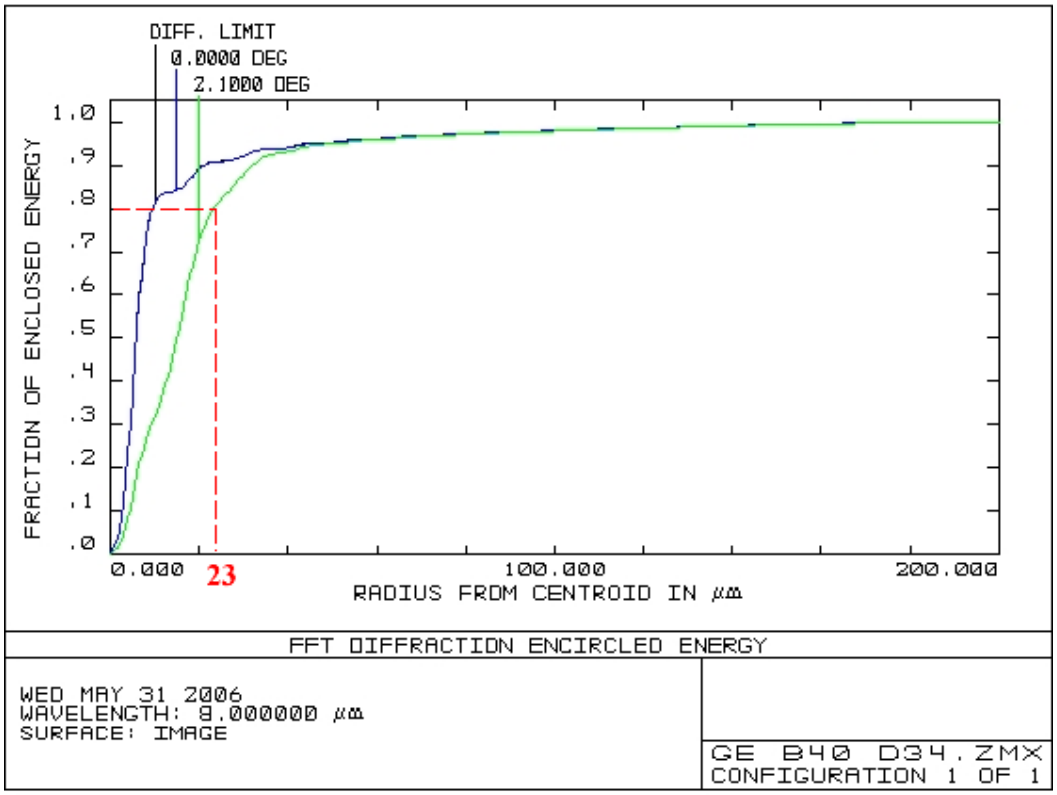

Figure 6.9 Encircled Energy

6.3.3 Modulation Transfer Function

MTF is one of the most useful means for characterizing the optical performance of an imaging system [27]. This presentation assumes that the object intensity is decomposed into its Fourier components [31]. The modulation transfer function data tell us how the modulation of the object is transferred from the object to the image as a function of the many varied spatial frequencies in the scene [27].

The quality of an optical system imaging a periodic object (which is varying sinusoidally in its intensity) can be determined from the image contrast. Contrast usually refers to the range of recognizable shades of gray between the dimmest and brightest parts of an object or image [41]. If $I_{\max}$ is the highest irradiance reading in the bar image and $I_{\min}$ is the lowest, the contrast or the modulation of the image is defined by [21, 27, 29]

$$Modulation = \frac{I_{\max} - I_{\min}}{I_{\max} + I_{\min}} \tag{6.15}$$

Modulation transfer function is the ratio of the modulation in the image to that in the object as a function of the spatial frequency. Spatial frequency is in cycles per unit length or in line pairs (one dark and one light line) per unit length, usually millimeter [21, 20].

$$MTF(v) = \frac{Modulation\ in\ image}{Modulation\ in\ object} \tag{6.16}$$

There exists one minimum spatial frequency in the object space whose amplitude is zero in the image space. This spatial frequency is referred to as the cutoff frequency, because the optical system images no spatial frequencies larger than this

one. For an aberration-free optical system with a circular aperture it is [21, 31, 27]:

$$\nu_{cutoff} = \frac{1}{\lambda(f/\#)} \tag{6.17}$$

From this equation, it can be stated that even a diffraction limited system (f/1) system in the LWIR cannot resolve more than 100 lp/mm.

Although high frequency cutoff may be one criterion for excellent performance it is not the only one. In some cases the systems in which the contrast remains higher at low frequencies at the expense of a high frequency cutoff can be preferred [29].

For the two-mirror system such as Cassegrain, the effect of obscuration must be considered when evaluating the image. Diffraction, as a result of the obscuration, increases the energy in the outer portions of the image at the expense of central bright spot. This reduces the MTF response of low spatial frequencies and increases the response at higher spatial frequencies [34].

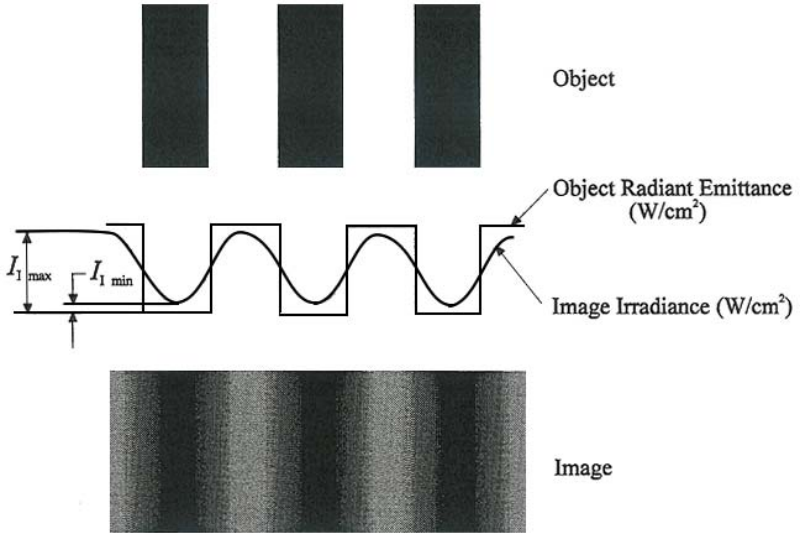

Figure 6.10 Modulation [21]

An infrared system is composed of many elements. Each of these components has a characteristic frequency response. One particular advantage of MTF is that the

frequency response of the entire system (or group of components) can be calculated by multiplying the responses of each component [42, 20]. MTF can include the effects of detector spatial response, electronics and optics and if applicable, display system. figure 6.11 gives a one-dimensional sketch of an example MTF and its components as a function of spatial frequency [43].

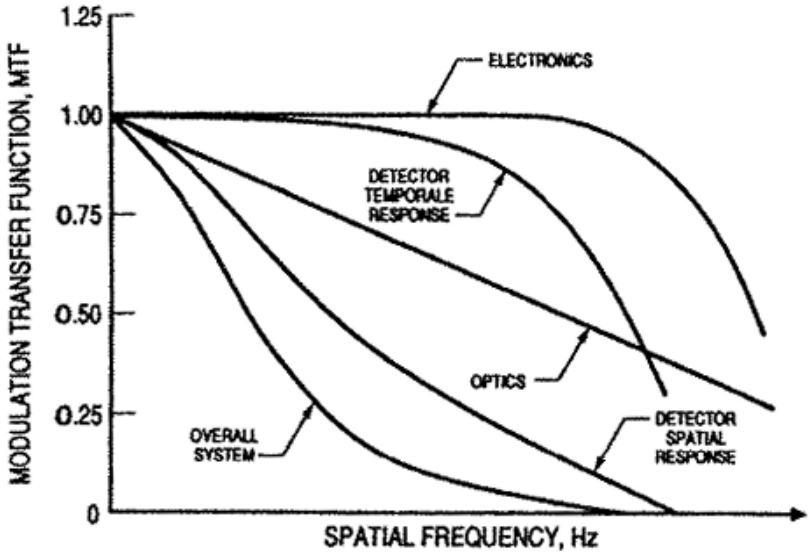

Figure 6.11 Individual components and the overall MTF of a sample sensor [43]

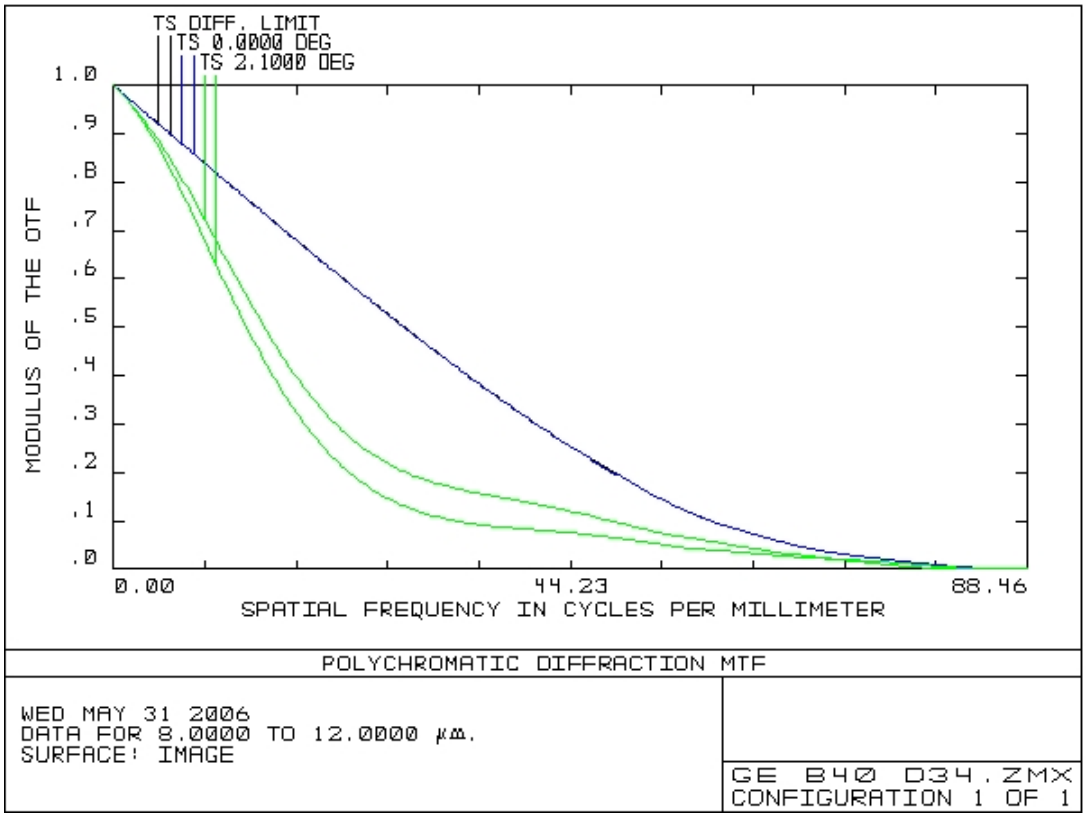

Figure 6.12 Diffraction Modulation Transfer Function for the designed system

As seen from the figure 6.12, MTF is computed or measures for bars that are radial and for bars that are tangential. These are orthogonal to each other [27]. The cutoff frequency is approximately 88.5 cycles per millimeter.

CHAPTER 7

DISCUSSION, CONCLUSION AND RECOMMENDATIONS FOR FUTURE WORK

In this study an optical design was made for a micro-satellite infrared imager at an altitude of 650 km with a mission of observing thermal changes, specifically forest fires on Earth's surface. From the examination of atmospheric effects, the spectral interval of the imager was determined to be 8.13–9.30μm to 10.3–12.5μm

The imager designed has a field of view FOV of 3.16 x 4.21 degrees, ground sample distance GSD of 300m and a ground coverage of 36km x 48km. These values are within the acceptable range defined by the space-borne fire recognition requirement criteria presented in tables 2.1 and 2.2.

However, the ground coverage of 36km x 48km is not sufficient to fullfill the requirement of short revisit time with a single micro-satellite. As it was mentioned in chapter 2, in a mission where the target signatures are rapidly varying, such as forest fires, short revisit times are required. This means it is desirable to have large ground coverage. Therefore, in order to perform a useful mission that intends to service in short revisit times, it is necessary to launch a number of satellites (constellation) with coordinated coverage and control.

The number of satellites to be launched depends on the ground coverage of a single satellite. The ground coverage can be increased by increasing the field of view of the optical system.

In this study, a Cassegrain type of reflective system configuration was selected. The field of view of reflective systems together with the baffling issues is rather limited compared to refractive systems. It is possible to design very flexible, wide FOV systems with refractive configurations. However, the difficulty of making an achromat system at a wide spectral region, coating and athermalization issues mentioned in part 4.3 and 4.4 becomes a crucial consideration in the refractive system design.Whereas, reflective systems does not encounter such difficulties. Considering the micro-satellite environmental conditions, making use of reflective surfaces was determined to be the most simple and stable solution.

Other important optical parameters were calculated as; effective focal length 100mm and optical aperture diameter of 70mm.Therefore the f/number, which is the ratio of effective focal length to entrance aperture diameter, is calculated to be 1.4. The Airy diameter is calculated to be 41.49 μm for this f/number. From the interpretation of spot diagrams, the rms radius is approximately 13 μm for the half field of 2.10 degrees meaning that all the rays are well within the Airy disk and the system is diffraction-limited. From the interpretation of encircled energy plot, %80 of the energy is contained within a diameter of 23μm which is a good match to the pixel pitch. The cutoff frequency is found to be approximately 88.5 cycles per millimeter.

For this study, an uncooled FPA with 160 x 120 pixels with 46 μm pixel pitch was determined to be suitable. This determination was made from the consideration of diffraction effects and resolution requirements. If higher resolution is required, the pixel size must be decreased. However, with the reduction of pixel size, the f/number must also be decreased to match the detector. For example for a working wavelength of 12μm, a

25μm pixel pitch size requires an f/number of 0.8 which is a very fast system and thus compelling for the correction of aberrations.

The recommendation for future work includes in-depth study of the optical coating issues. As it was mentioned in chapter 4.3, anti-reflection coating is obligatory especially for infrared refractive surfaces, for this case the germanium used as a corrector that encounter high reflection losses. Mirror surfaces also require metalic coating to provide the surface high reflectivity throughout the desired spectrum.

Another consideration is the thermal gradient faced by the interior of a micro-satellite (see chapter 4.3.2). The 10 degree C variation over the orbit will mostly effect the thin germanium corrector and cause an amount of focus shift due to the change of refractive index with temperature. This effect has to be simulated in order to see if the amount of shift is considerable or not. If it is, thermal compensation (athermalization) is required.

It is also strongly recommended that further performance evaluations are to be made by the inclusion of a commercial-off-the-shelf detector. The optical system is not a stand alone system and the performance analysis of the optical system may not reflect or give an idea of the performance level of the entire system. Further system analysis has to made including a commercial-off-the-shelf detector manufacturer data. With the necessary SNR calculations, more realistic assessment can be made. It is also important to follow and consider the rapid developments in the uncooled and cooled infrared detector technologies.

REFERENCES

1. Wolfe,William L., *Introduction to Infrared System Design*, SPIE Optical Engineering Press , 1996
2. Oelrich Brian D., Dr. Craig Underwood, *Low Cost Thermal IR Imager for an Earth Observation Micro-satellite*, 2004
3. Oelrich Brian D., *The Design and Characterization of a Low-cost Micro-satellite Thermal IR Imager Based on COTS Technology*, PhD thesis, University of Surrey, 2005
4. MODIS Website, *http://modis.gsfc.nasa.gov/* , [last accessed date: 26 June 2006]
5. The International Space University's Small Satellite Interdisciplinary Survey (ISIS) Homepage, *http://mss01.isunet.edu/isis/* , [last accessed date: 26 June 2006]
6. Grillmayer G., Lengowski M., Walz S. et. al., *Flying Laptop- Micro-satellite of the University of Stuttgart For Earth Observation and Technology Demonstration* , Proceedings of IAC 2004, Vancouver, Canada, Oct. 4-8, 2004
7. Schowengerdt Robert, *Remote Sensing: Models and Methods for Image Processing*, Academic Press, 1997
8. GAF Remote Sensing and Geoinformation Systems Website, *http://www.gaf.de/presshelp/index1.htm*, [last accessed date: 26 June 2006]
9. GIS Development: The Geospatial Resource Portal Website, *http://www.gisdevelopment.net/tutorials/tuman008.htm* , [last accessed date: 26 June 2006]
10. Leachtenaur Jon C., Driggers Ronald G., *Surveillance and Reconnaissance Imaging Systems-Modeling and Performance Prediction*, Artech House Inc., 2001

11. Driggers Ronald G.,Cox Paul ,Edwards Timothy, *Introduction to Infrared and Electro-Optical Systems,* Artech House Optoelectronics Library,1998

12. Lomheim T.S., Milne, E.L., Kwok, J.D., Tsuda, A., *Performance/Sizing Relationships for a Detection Space Sensor Short-waveMid-wave Infrared Scanning Point-Source,* Aerospace Conference Proceedings, 6-13 March 1999 113 - 138 vol.4 Aspen, CO

13. The Eurostat Concepts and Definitions Database Webpage, *http://forum.europa.eu.int/irc/dsis/coded/info/data/coded/en/gl009971.htm*, [last accessed date: 26 June 2006]

14. The University of Texas Department of Geological Sciences Website *http://www.geo.utep.edu/pub/keller/Resolution/Resolution.html* , [last accessed date: 26 June 2006]

15. Canada Centre for Remote Sensing Homepage, *http://ccrs.nrcan.gc.ca/resource/tutor/fundam/chapter2/03_e.php*, [last accessed date: 26 June 2006]

16. Dudzik Micheal C. (editor), *The Infrared and Electro-Optical Systems Handbook,Volume 4, Electro-Optical Systems Design, Analysis, and Testing*, SPIE Optical Engineering Press, 1993

17. Surrey Space Centre Small Satellites Home Page, *http://www.smallsatellites.org*, [last accessed date: 26 June 2006]

18. Holst Gerald C., *Testing and Evaluation of Infrared Imaging Systems Second Edition*, Jcd Publishing, 1998

19. Holst Gerald C., *Elecro-optical Imaging System Performance*, Jcd Publishing, 2000

20. Smith Warren J., *Modern Optical Engineering, Third Edition*, Mc-Graw-Hill Inc, 2000

21. Riedl Max J.,*Optical Design Fundamentals for Infrared Systems,* Second Edition, SPIE Press, 2001

22. The Air Force Research Lab, Space Vehicles Directorate *http://www.vs.afrl.af.mil/ProductLines/IR-Clutter/modtran4.aspx*, [last accessed date: 26 June 2006]

23. Uttamchandani Deepak, Andonovic Ivan, *Principles of Modern Optical Systems Volume 2* , Artech House, 1992

24. Rogatto William D.(editor), *The Infrared and Electro-Optical Systems Handbook, Volume 3, Electro-Optical Components*, SPIE Optical Engineering Press, 1993

25. Schlessinger Monroe, *Infrared Technology Fundamentals ,Second Edition Revised and Expanded*, Marcel Dekker Inc., 1995

26. Jenkins Francis A.,White Harvey E., *Fundamentals of Optics*, Mcgraw-Hill College, 4th edition 1976

27. Fisher,Robert E., Biljana Tadic-Galep, *Optical System Design*, SPIE Press-McGrawhill, 2000

28. Pedrotti Frank L. S.L.,Pedrotti Leno S., *Introduction to Optics ,Second Edition,* Prentice-Hall International Inc, 1993

29. O'shea Donald, *Elements of Modern Lens Design*, John Wiley and Sons Publication, 1985

30. Meyer-Arendt Jurgen R., *Introduction to Classical and Modern Optics, Fourth Edition*, Prentice-Hall International, 1995

31. Malaraca Daniel, Thompson Brian J., Handbook of Optical Engineering, Marcel Dekker Inc., 2001

32. Mann Allen, *Infrared Optics and Zoom Lenses*, SPIE Press, 2000

33. Wolfe William L., *Optical Engineer's Desk Reference*, Optical Society of America, 2003

34. Laikin Milton , *Lens Design, Second Edition Revised and Expanded*, Marcel Dekker Inc., 1995

35. Bely Pierre , *Design and Construction of Large Optical Telescopes*, Yves Springer Verlag, 2003

36. Jha A. R., *Infrared Technology - Application to Elecrooptics, Photonic Devices, and Sensors,* Wiley and Sons Inc., *2000*

37. Federation of American Scientists (FAS) ES310 Introduction to Naval Weapons Engineering, Electro-Optical Imaging Systems Webpage, *http://www.fas.org/man/dod-01/navy/docs/es310/EO_image/EO_Image.htm* [last accessed date: 26 June 2006]

38. Schroeder Daniel J., *Astronomical Optics, Second Edition,* Academic Press, 2000

39. Texereau Jean, *How to make a Telescope*, *Second English Edition*, Willmann-Bell Inc., 1984

40. Smith Warren J., *Modern Lens Design: A Resource Manual*, McGraw-Hill Inc., 1992

41. Williams Charles S., Becklund Orville A., *Introduction to the Optical Transfer Function*, John Wiley & Sons, 1989

42. Holst Gerald C., *Common Sense Approach to Thermal Imaging*, SPIE Press, 2000

43. Seyrafi Khalil,Hovanessian S.A., *Introduction to Electro-Optical Imaging and Tracking Systems*, Artech House, Incorporated, 1993

44. I. Walter, K Brieß, et al., *BIRD - Microsatellite for Hot Spot Detection* , Proceedings of the 13th AIAA/USU Conference on Small Satellites, Logan UT, Aug. 23-26, 1999

45. Brieß K., Bärwald W., Gill E., et al., *Technology Demonstration by the BIRD Mission*, Acta Astronautica 56, 2005

46. Zemax Optical Design Program (Focus Software), *User's Guide*, Nov. 2005

47. Melles Griot Homepage, *http//www.mellesgriot.com,* [last accessed date: 26 June 2006]

48. Wolfe William , Zissis G. J., *Infrared Handbook*, ERIM, 1978

APPENDIX A

BASIC OPTICAL DEFINITION OF TERMS

There are some terms which are often used in this study. Optical system characteristics can be defined by its 6 cardinal points consisting of the first and second *focal points* (F_1 and F_2) , the first and second *principal points* (H_1 and H_2) and the first and second *nodal points* (N_1 and N_2) [2]. The focal points are those points at which light rays parallel to the optical axis are brought to a common focus on the axis. The intersection of principal planes with the optic axis is the principal point. The “second” focal point and the “second” principal point are those defined by rays approaching the system from the left. The “first” points are those defined by rays from the right. The nodal points are two axial points such that a ray directed toward the first nodal point appears (after passing through the system) to emerge from the second nodal point parallel to its original direction [20].

The effective focal length (efl) of a system is the distance from the principal point to the focal point. The *back focal length (bfl),* or back focus, is the distance from the vertex of the last surface of the system to the second focal point. The *front focal length (ffl)* is the distance from the front surface to the first focal point [20].

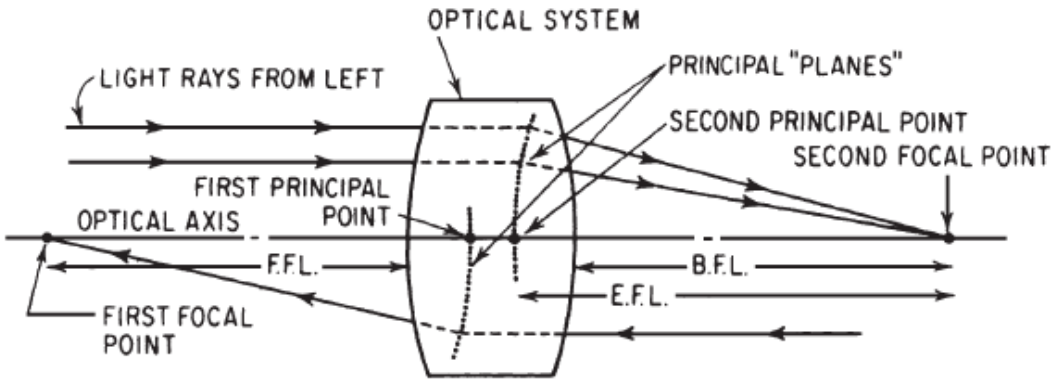

Figure A.1 Location of the focal and principal points of the optic system [20]

Aperture Stop of an optical system is the actual optical component that limits the size of the maximum cone of rays from an axial object point that can be processed by the entire system. Thus it controls the brightness of the image [28].

The *entrance and exit pupils* of the system are the images of the aperture stop in object and image space, respectively. That is, the entrance pupil is the image of the aperture stop as it would be seen if viewed from the axial point on the object; the exit pupil is the aperture stop image as it would be seen if viewed from the final image plane [20].

Chief Ray is defined to be the ray that travels from a specific field point, through the center of entrance pupil and on to the image surface [46].

Tangential plane, for typical rotationally symmetric systems, is the YZ plane and *sagittal plane* is the plane orthogonal to the YZ plane which intersects the center of the Entrance Pupil [46].

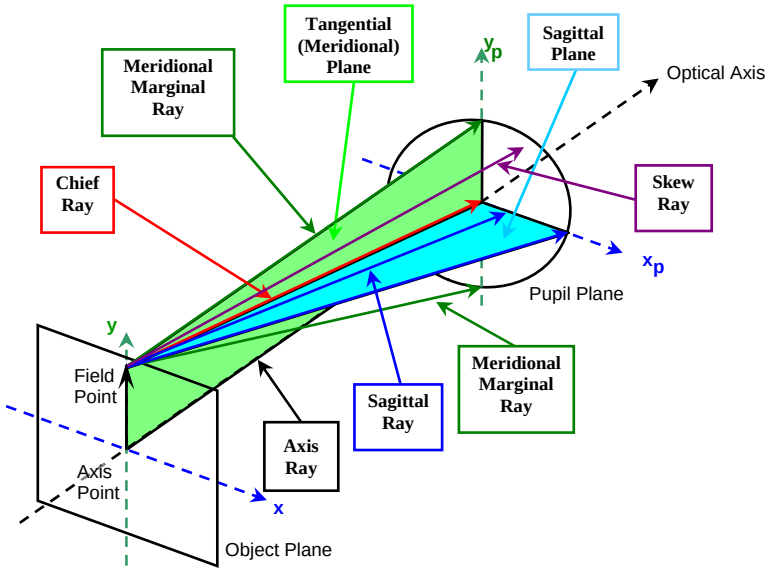

Figure A.2 Chief Ray, Meridional and Sagittal Planes [47]

Field stop is the aperture that controls the field of view by limiting the solid angle formed by chief rays [28]. The field stop is a device that blocks rays that are beyond its dimensions from reaching the detecting element(s). If there is no physical stop, then the boundaries of the detecting elements determine the field stop dimensions.

Entrance Window is the image of the field stop formed by all optical elements preceding it. *Exit Window*, analogous to the exit pupil, is the image of the field stop formed by all optical elements following. Since these two planes are both images of the field stop, they are conjugate planes [28].

F-number (f/#) or *relative aperture* is the ratio of the focal length to the clear aperture of a lens system. When a lens forms the image of an extended object, the amount of energy collected from a small area of the object is directly proportional to the area of the clear aperture, or entrance pupil, of the lens. At the image, the

illumination (power per unit area) is inversely proportional to the image area over which this object is spread. The aperture area is proportional to the square of the pupil diameter, and the image area is proportional to the square of the image distance, or focal length. Thus, the square of the ratio of these two dimensions is a measure of the relative illumination produced in the image. The illumination in an image is inversely proportional to the square of f/number [20].

$$f/\# = \frac{effective\ focal\ length}{clear\ aperture\ diameter} \tag{A.1}$$

Working F/# is defined as [46],

$$W = \frac{1}{2n\sin\theta} \tag{A.2}$$

Where θ the real marginal ray angle in image space and n is is the index of refraction of image space. It is based upon real ray data at the actual conjugates of the lens [46].

Numerical aperture is the index of refraction (of the medium in which the image lies) times the sine of the half angle of the cone of illumination.

$$Numerical\ Aperture = NA = n.\sin u \tag{A.3}$$

For aplanatic systems the two quantities are related by [46]

$$f/number = \frac{1}{2NA} \tag{A.4}$$

APPENDIX B

OPTICAL MATERIALS FOR INFRARED

Figure B.1 shows transmission region of most infrared optical materials. The limiting wavelengths chosen are those at which a sample of 2mm thickness has %10 external transmittance [48]."*External Transmittance*" is the measured value of a sample including reflection losses [24].

A bar with straight vertical ending indicates that the cutoff exist at the wavelength represented by the end of the bar, a bar with an S-shape ending represents a material which cuts off at approximately at that wavelength, a bar ending in an angle indicates that material transmits at least to that wavelength, and probably further.[48]

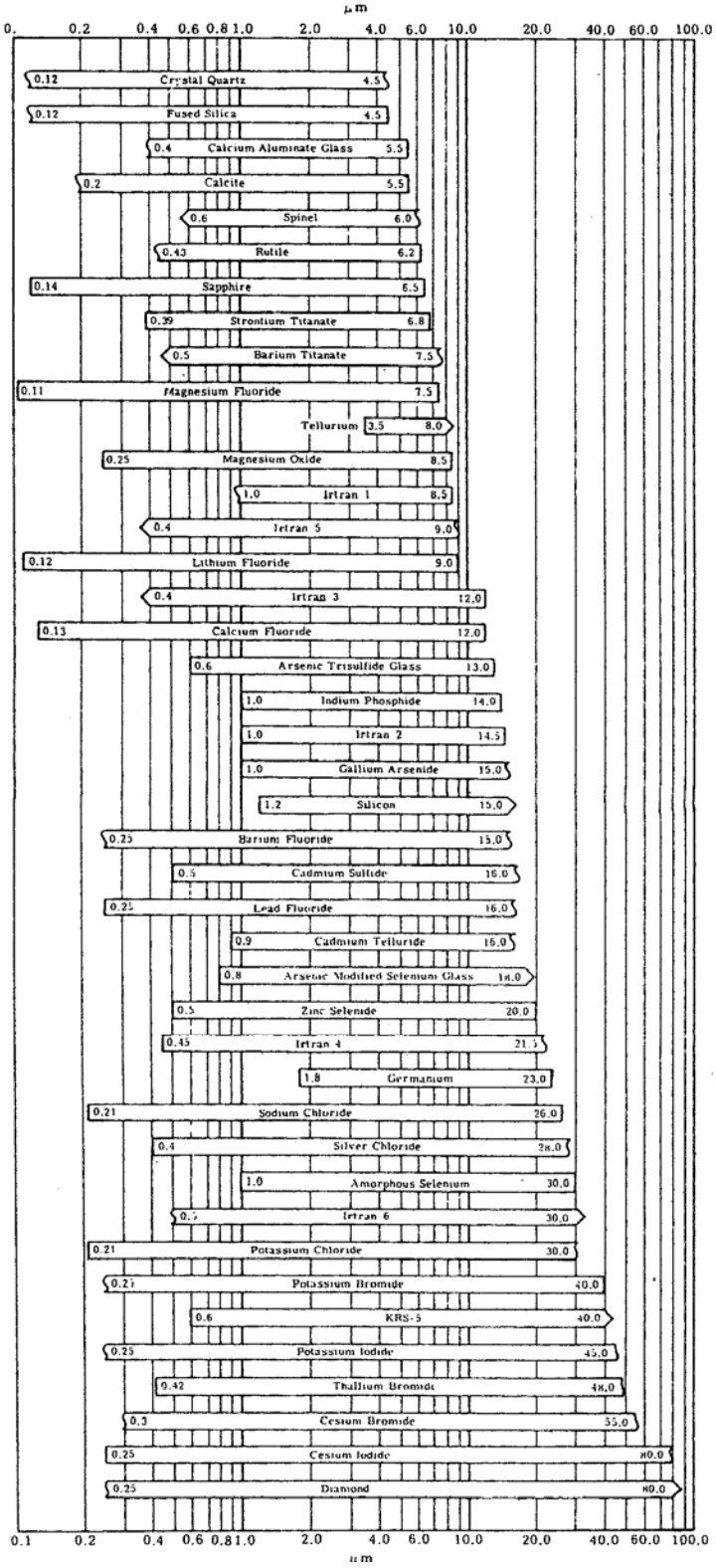
μm
0. 0.2 0.4 0.6 0.8 1.0 2.0 4.0 6.0 10.0 20.0 40.0 60.0 100.0
0.12 Crystal Quartz 4.5
0.12 Fused Silica 4.5
0.4 Calcium Aluminate Glass 5.5
0.2 Calcite 5.5
0.6 Spinel 6.0
0.43 Rutile 6.2
0.14 Sapphire 6.5
0.39 Strontium Titanate 6.8
0.5 Barium Titanate 7.5
0.11 Magnesium Fluoride 7.5
Tellurium 3.5 8.0
0.25 Magnesium Oxide 8.5
1.0 Irtran 1 8.5
0.4 Irtran 5 9.0
0.12 Lithium Fluoride 9.0
0.4 Irtran 3 12.0
0.13 Calcium Fluoride 12.0
0.6 Arsenic Trisulfide Glass 13.0
1.0 Indium Phosphide 14.0
1.0 Irtran 2 14.5
1.0 Gallium Arsenide 15.0
1.2 Silicon 15.0
0.25 Barium Fluoride 15.0
0.5 Cadmium Sulfide 16.0
0.25 Lead Fluoride 16.0
0.9 Cadmium Telluride 16.0
0.8 Arsenic Modified Selenium Glass 18.0
0.5 Zinc Selenide 20.0
0.45 Irtran 4 21.5
1.8 Germanium 23.0
0.21 Sodium Chloride 26.0
0.4 Silver Chloride 28.0
1.0 Amorphous Selenium 30.0
0.7 Irtran 6 30.0
0.21 Potassium Chloride 30.0
0.25 Potassium Bromide 40.0
0.6 KRS-5 40.0
0.25 Potassium Iodide 45.0
0.42 Thallium Bromide 48.0
0.3 Cesium Bromide 55.0
0.25 Cesium Iodide 80.0
0.25 Diamond 80.0
0.1 0.2 0.4 0.6 0.8 1.0 2.0 4.0 6.0 10.0 20.0 40.0 60.0 100.0
μm

Figure B.1 Transmission regions of optical materials (2mm thickness) [48]*

Samples of spectral curves of external transmittance are given in figures B.2 through B.6.

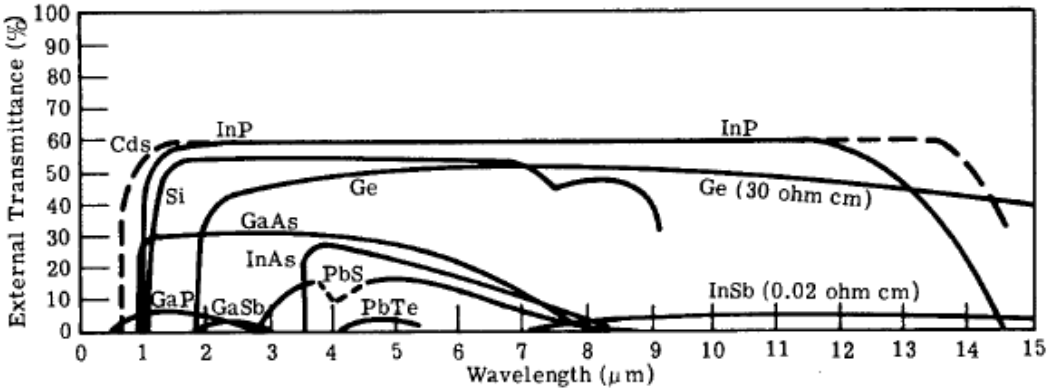

Figure B.2 The transmission of cadmium sulfide, indium phosphide, silicon, germanium, gallium arsenide, gallium phosphide, gallium antimonide, indium arsenide, indium antimonide lead telluride and lead sulfide [24]

* Irtran 6 is no longer manufactured by the Eastman Kodak Co. Irtran ® is a registered trademark of the Eastman Kodak Co.

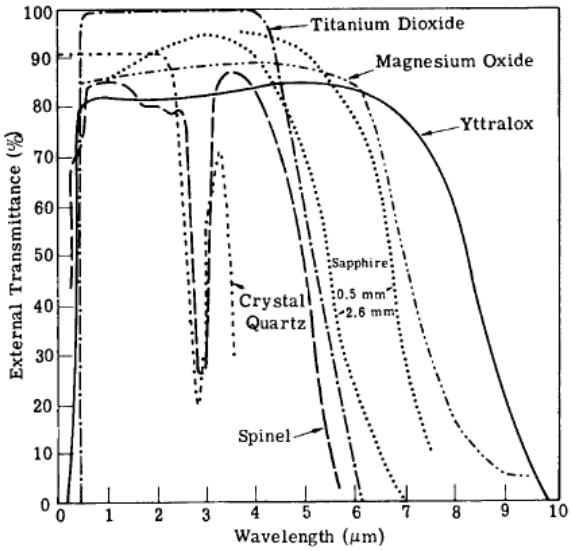

Figure B.3 The transmission of sapphire, spinel, titanium dioxide, crystal quartz (for the ordinary ray), Yttralox, and magnesium oxide[24].

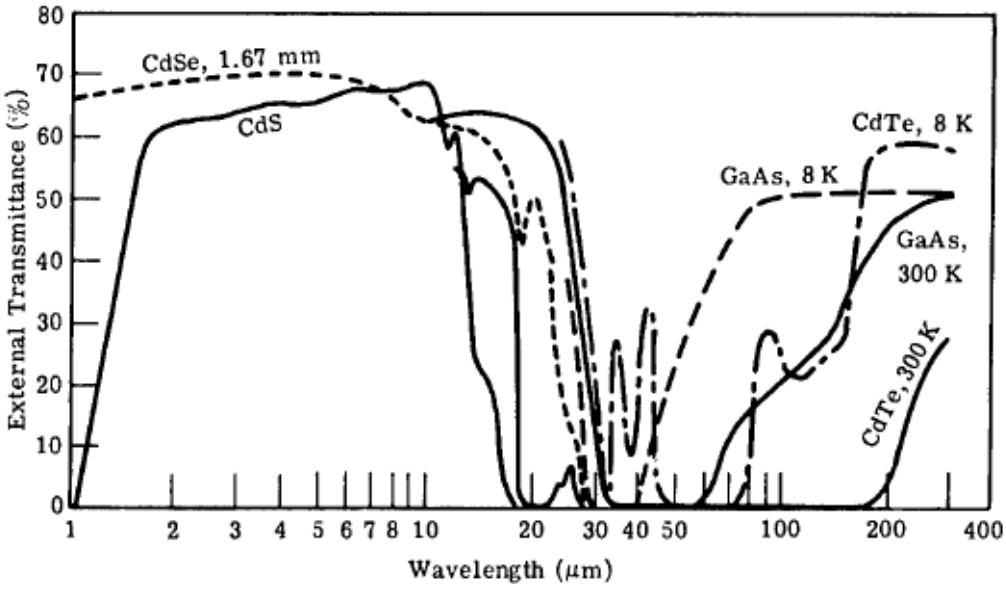

Figure B.4 The transmission of cadmium sulfide, cadmium telluride, gallium arsenide, and cadmium selenide [24]

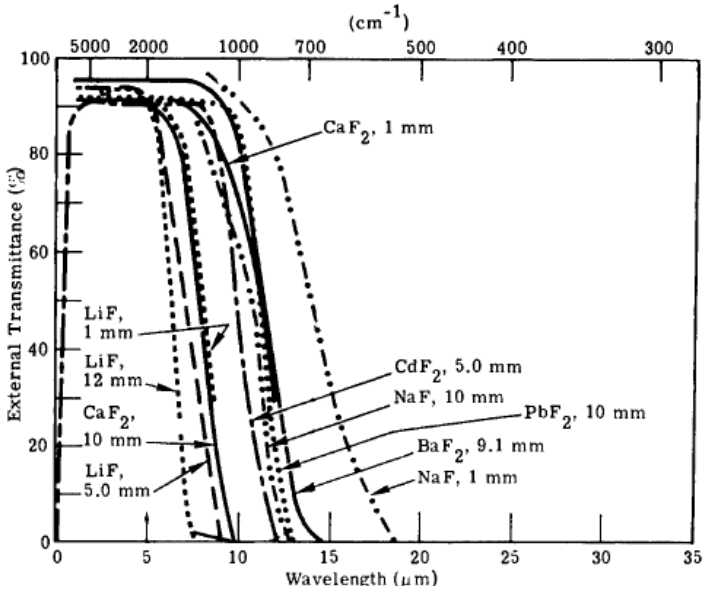

Figure B.5 The transmission of barium fluoride, cadmium fluoride, lithium fluoride, calcium fluoride, lead fluoride, and sodium fluoride [24]

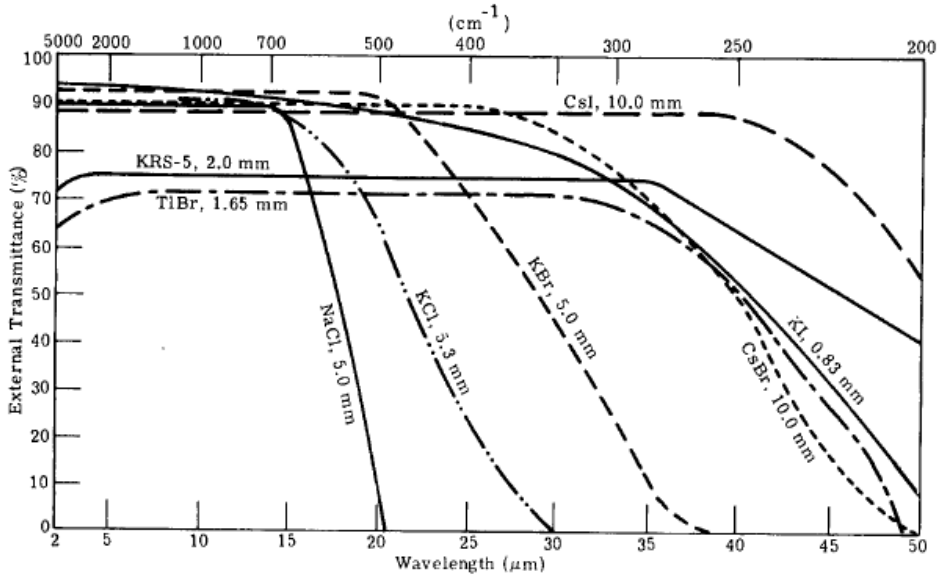

Figure B.6 The transmission of cesium iodide, potassium iodide, potassium bromide, thallium bromide, KRS-5, cesium bromide, sodium chloride, and potassium chloride [24]

Germanium has been one of the most used infrared optical materials. It has a spectacularly high refractive index value of about 4 and a concomitant, low dispersion. The equivalent Abbe number in the 3 to 5 μm region is 101, and in the 8 to 12 μm region it is 990. The refractive index value reported by Li, Herzberger and Salzburg are shown in Table B.1.

Table B.1 Refractive index values for Germanium [24]

Wavelength	Index		
	Li	Herz	Salz
2.0581	4.1239	4.1016	4.1016
2.1526	4.1133	4.0920	4.0919
2.3126	4.0981	4.0787	4.0786
2.4374	4.0882	4.0702	4.0708
2.577	4.0789	4.0622	4.0609
2.7144	4.0710	4.0557	4.0552
2.998	4.0580	4.0450	4.0452
3.3033	4.0475	4.0366	4.0369
3.4188	4.0443	4.0340	4.0334
4.258	4.0280	4.0214	4.0216
4.866	4.0210	4.0161	4.0170
6.238	4.0121	4.0093	4.0094
8.66	4.0055	4.0044	4.0043
9.72	4.0040	4.0034	4.0034
11.04	4.0027	4.0026	4.0026
12.2	4.0019	4.0022	4.0023
13.02	4.0015	4.0021	4.0021
14.21	4.0010	4.0022	4.0015
15.08	4.0007	4.0024	4.0014
16	4.0004	4.0028	4.0012

Figure B.7 presents curves of refractive index versus wavelength and illustrates the range of the refractive indices of many of the materials.

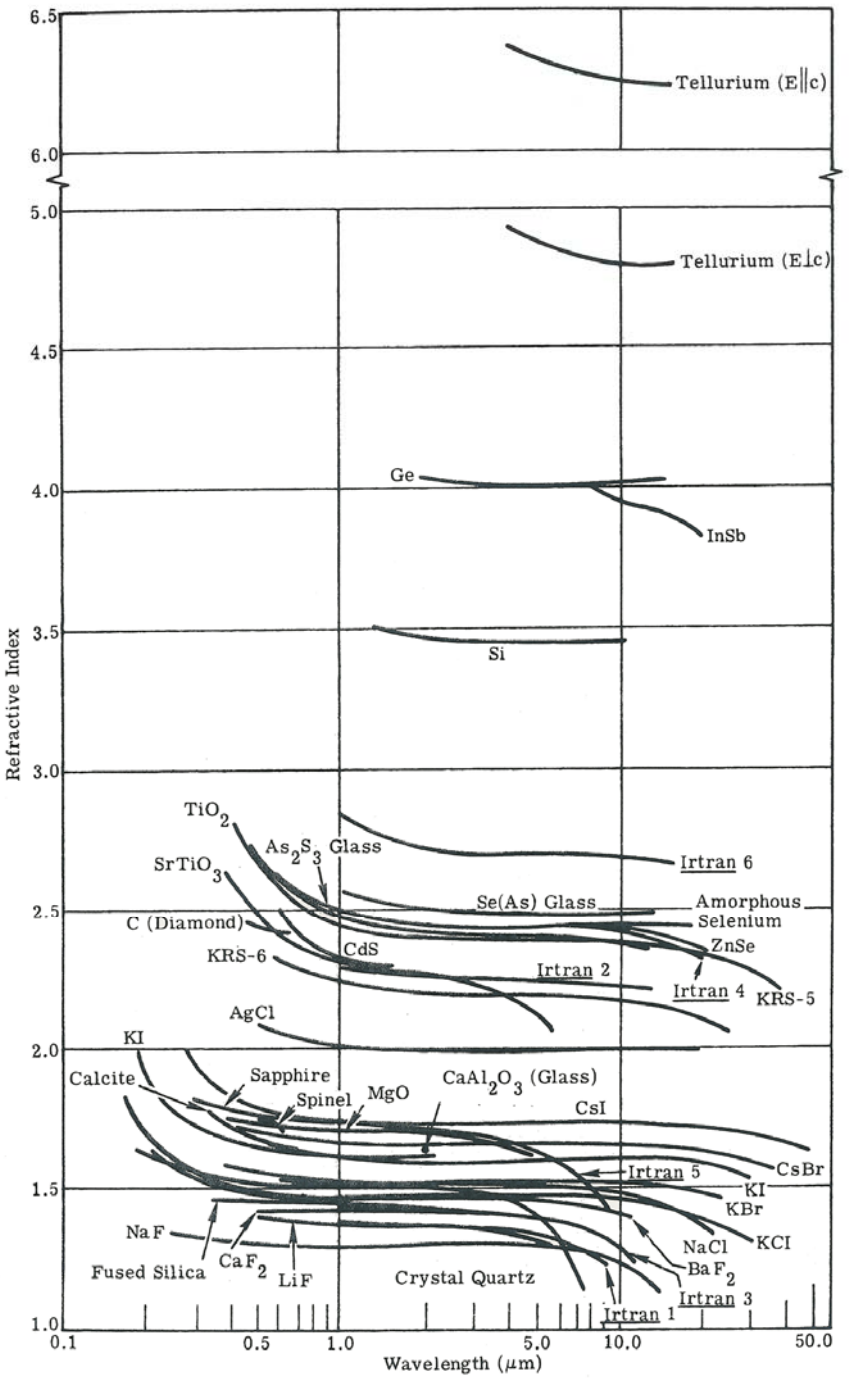

Figure B.7 Refractive index values [48]

The data of figure B.7 are plotted in figure B.8 to show the rate of change of the refractive index versus wavelength. [48]

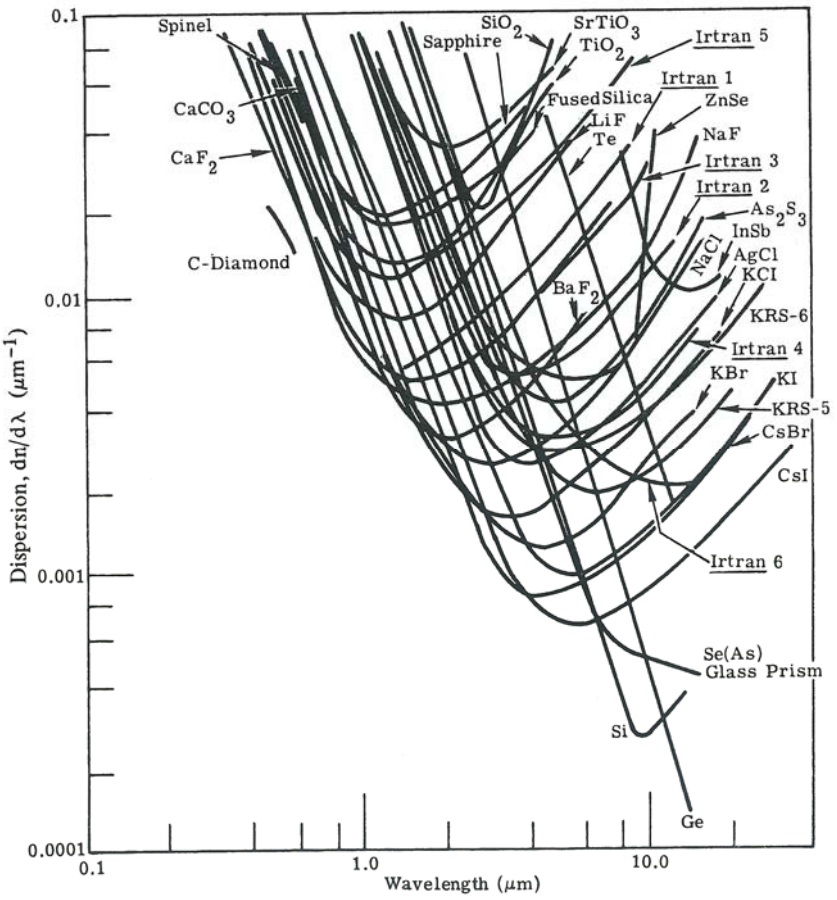

Figure B.8 *dn/dt* versus λ for selected materials[48]

APPENDIX C

PRESCRIPTION DATA

Table C1. General Lens Data

Surfaces	7
Stop	3
System Aperture	Entrance Pupil Diameter = 70
Glass Catalogs	SCHOTT INFRARED
Ray Aiming	Off
Apodization	Uniform, factor = 0.00000E+000
Effective Focal Length	98.78445 (in air at system temperature and pressure)
Effective Focal Length	98.78445 (in image space)
Back Focal Length	2.308716
Total Track	65.42872
Image Space F/#	1.411206
Working F/#	1.413443
Image Space NA	0.3339645
Object Space NA	3.5e-009
Stop Radius	35
Paraxial Image Height	3.622261
Entrance Pupil Diameter	70
Entrance Pupil Position	58
Exit Pupil Diameter	138.5794
Exit Pupil Position	195.5641
Field Type	Angle in degrees
Maximum Field	2.1
Primary Wave	12
Lens Units	Millimeters
Angular Magnification	-0.5051256

Table C2. Index of Refraction Data

Surf	Glass	Temp	Pres	8.000000	10.0000000	12.0000000
0		20.00	1.00	1.00000000	1.00000000	1.00000000
1		20.00	1.00	1.00000000	1.00000000	1.00000000
2		20.00	1.00	1.00000000	1.00000000	1.00000000
3	MIRROR	20.00	1.00	1.00000000	1.00000000	1.00000000
4	MIRROR	20.00	1.00	1.00000000	1.00000000	1.00000000
5	GERMANIUM	20.15	1.00	4.00675003	4.00437994	4.00291403
6		20.00	1.00	1.00000000	1.00000000	1.00000000
7		20.00	1.00	1.00000000	1.00000000	1.00000000

Table C3. Edge Thickness Data

Surf	Edge
1	24.705416
2	24.809788
STO	-26.187818
4	38.182797
5	2.552754
6	1.365779
IMA	0.000000

Table C4. F/# Data

F/# calculations consider vignetting factors and ignore surface apertures.

	Wavelength:	8.000000		10.000000		12.000000	
#	Field	Tan	Sag	Tan	Sag	Tan	Sag
1	0.0000 deg:	1.4131	1.4131	1.4133	1.4133	1.4134	1.4134
2	2.1000 deg:	1.4995	1.4376	1.4996	1.4377	1.4997	1.4379

Table C4. Cardinal Points

Object space positions are measured with respect to surface 1. Image space positions are measured with respect to the image surface. The index in both the object space and image space is considered.

		Object Space	Image Space
W = 8.000000			
Focal Length	:	-98.759321	98.759321
Focal Planes	:	108.554338	-0.000290
Principal Planes	:	207.313658	-98.759611
Anti-Principal Planes	:	9.795017	98.759031
Nodal Planes	:	207.313658	-98.759611
Anti-Nodal Planes	:	9.795017	98.759031
W = 10.000000			
Focal Length	:	-98.774842	98.774842
Focal Planes	:	108.149177	-0.000111
Principal Planes	:	206.924019	-98.774953
Anti-Principal Planes	:	9.374335	98.774731
Nodal Planes	:	206.924019	-98.774953
Anti-Nodal Planes	:	9.374335	98.774731
W = 12.000000 (Primary)			
Focal Length	:	-98.784446	98.784446
Focal Planes	:	107.898555	0.000000
Principal Planes	:	206.683001	-98.784446
Anti-Principal Planes	:	9.114109	98.784446
Nodal Planes	:	206.683001	-98.784446
Anti-Nodal Planes	:	9.114109	98.784446